Optimizing Rainfall-Triggered Landslide Thresholds to Warning Daily Landslide Hazard in Three Gorges Reservoir Area

Bo Peng[1], Xueling Wu[1]

[1]School of Geophysics and Geomatics, China University of Geosciences, Wuhan 430074, China

Correspondence to: Xueling Wu (wuxl@cug.edu.cn)

Abstract. Rainfall is intrinsically ~~connected~~linked to the ~~incidence~~occurrence of landslide catastrophes. ~~Exploring~~Identifying the ~~ideal~~most suitable rainfall threshold model ~~(RTM)~~ for an area ~~in order to determine the rainfall warning level (RWL)~~is crucial for ~~the region~~establishing effective daily landslide hazard warnings, which are essential for ~~daily landslide hazard warning (LHW) is critical for~~the precise prevention and management of local landslides. ~~In this paper, a method for calculating rainfall thresholds using~~ This study introduces a novel approach that utilizes multilayer perceptron (MLP) regression ~~is proposed~~ to calculate rainfall thresholds for 453 rainfall-induced landslides. ~~First, the study area was divided into subareas based on topography and climate conditions. Then, two methods,~~This research represents the first attempt to integrate MLP and ordinary least squares ~~(OLS), were utilized to explore~~methods for determining the optimal ~~RTM for each subregion. Subsequently, 11 factors along with three models were selected to predict landslide susceptibility (LS). Finally, to obtain daily LHW result for the study area, a superposition matrix was employed to overlay the daily RWL with the ideal LS prediction results. The following are the study's findings: (1) The optimal RTMs and calculation methods are different for different~~rainfall threshold model tailored to distinct subregions~~. (2) The Three~~, categorized by topographical and climatic conditions. Additionally, an innovative application of a three-dimensional convolutional neural network ~~model produces more accurate LS prediction results.~~(CNN-3D) model is introduced to enhance the accuracy of landslide susceptibility predictions. Finally, a comprehensive methodology is developed to integrate daily rainfall warning levels with landslide susceptibility predictions using a superposition matrix, thus offering daily landslide hazard warning results for the study area. The key findings of this study are as follows: (1) The optimal rainfall threshold models and calculation methods vary across different subregions, underscoring the necessity for tailored approaches. (2) The CNN-3D model substantially improves the accuracy of landslide susceptibility predictions. (3) The daily ~~LHW was~~ landslide hazard warnings were validated using anticipated rainfall data ~~for~~from July 19, 2020, thereby demonstrating the reliability of both the landslide hazard warning results and the ~~validation results proved the correctness of~~ rainfall threshold model. This study presents a substantial advancement in the ~~LHW results~~ precise prediction and ~~RTM~~management of landslide hazards by employing innovative modeling techniques.

1 Introduction

~~Landslide catastrophes~~According to the China Statistical Yearbook, landslides accounted for 71.55% of geological disasters in China ~~from~~between 2005 ~~to~~and 2021~~, according to the China Statistical Yearbook~~ (http://www.stats.gov.cn/sj/ndsj/). Frequent ~~landslide catastrophes endanger people's~~landslides pose significant risks to both lives and property (Xing et al., 2021). Rainfall ~~will lead to landslide disasters~~triggers landslides by ~~changing the~~altering pore pressure in the soil ~~body~~ (Zhao et al., 2022) and ~~weakening~~reducing the shear strength of the geotechnical ~~body~~materials (Chan et al., 2018). ~~According to research (Marin et al., 2020; Yuniawan et al., 2022):~~Research indicates that rainfall is intrinsically ~~connected~~linked to the ~~great~~ majority of landslide ~~deformation and instability.~~deformations and instabilities(Marin et al., 2020; Yuniawan et al., 2022). Therefore, it is ~~significant~~crucial to delineate the rainfall thresholds for ~~different rainfall~~various conditions and ~~areas through the study for the fine development of~~regions to improve landslide hazard ~~warning (LHW)~~warnings and disaster prevention ~~and control. LHW~~ efforts. Landslide hazard warning is described as the conditional prediction of ~~probable landslide~~ the temporal and spatial ~~probability under the limitations of~~probabilities of landslide occurrence based on triggering and inducing ~~variables~~factors (Budimir et al., 2015). ~~The~~ In this study, the rainfall warning level (~~RWL) (~~i.e., the temporal probability of landslide occurrence) ~~calculated by~~derived from the rainfall threshold model ~~(RTM) is~~serves as the triggering factor~~ in this study, and~~, while the landslide susceptibility predictions (i.e., the spatial probability of occurrence) act as the inducing factor~~ is the prediction result of landslide~~.

Landslide susceptibility ~~(LS) (i.e.,~~reflects the spatial probability of landslide occurrence~~) calculated by the susceptibility model.The spatial probability of landslide occurrence can be reflected by LS~~ (Huang et al., 2022b). ~~General~~Methods for predicting landslide susceptibility include general linear models (Aksha et al., 2020), information value models (Yu et al., 2022), and various machine learning models~~, and others are among the methods used to predict LS.~~. Machine learning models ~~can fit~~are more effective than other types in capturing and ~~predict~~predicting the nonlinear ~~relationship~~relationships between ~~LS and~~ landslide susceptibility and predisposing factors~~ more effectively than other kinds of models~~ (Guo et al., 2021). Commonly used machine learning models include logistic regression (Baharvand et al., 2020), artificial neural networks (Jiang et al., 2014), support vector machines (SVM) (Chang et al., 2023; Zhu and Hu, 2012), random forests (RF) (Chen et al., 2014; Huang et al., 2024), Bayesian algorithms (He et al., 2019), and deep learning algorithms (Huang et al., 2020). However, ~~determining which~~selecting the most suitable model ~~is best suited~~ for ~~LS~~landslide susceptibility prediction ~~is~~remains challenging, and ~~there is great~~significant uncertainty exists in the ~~LS prediction~~ results ~~of various~~obtained from different machine learning models (Xia et al., 2020). Even ~~little~~small improvements in ~~LS~~ prediction accuracy ~~might have a significant influence on LS~~ can significantly impact landslide susceptibility zoning (Chen et al., 2018). Therefore, to ~~decrease the~~reduce uncertainty ~~of LS~~in landslide susceptibility results, ~~different~~multiple susceptibility models are ~~frequently employed to predict LS in the study area~~often applied, and the model with the ~~greatest~~highest accuracy is ~~chosen~~selected for the study area.

~~RTM~~Rainfall threshold modeling approaches primarily include of deterministic methods based on physical and hydrological models, as well as empirical methods based on landslide cataloguing and rainfall event statistics (Chung et al., 2017; Wu et al., 2015). ~~The former establishes~~Deterministic methods establish the relationship between rainfall and landslide stability through dynamic hydrological models and ~~determines~~determine the critical rainfall threshold for landslide instability ~~in the physical model~~ (Ciurleo et al., 2019). However, due to the ~~difficulty in~~challenges of accurately obtaining hydrological ~~parameters~~ and geotechnical parameters on a large scale, this method is ~~only~~primarily applicable to smaller study ~~area~~areas (Wu and Yeh, 2020). ~~The latter is~~Empirical methods are mainly derived by calculating the relationship between historical landslide and rainfall data (Abraham et al., 2020a; Pradhan et al., 2019). This ~~method~~approach is widely used ~~because of~~due to its advantages ~~of convenience~~ in data acquisition~~, strong~~ convenience, applicability, and ~~excellent results~~effectiveness (Martinovic et al., 2018). ~~Currently, commonly~~Commonly used ~~RTM~~rainfall threshold models include the intensity~~ of rainfall -~~-duration~~ of rainfall~~ (I-D) threshold model (Abraham et al., 2019; Lee et al., 2014) and the effective rainfall~~ -~~-duration of rainfall (E-D) threshold model (Abraham et al., 2020b; Peruccacci et al., 2017). ~~The regression~~Regression methods used to calculate the ~~RTM~~rainfall threshold model include logistic regression (Mathew et al., 2014), ordinary least squares (OLS) regression (Rossi et al., 2017) and quantile regression (Salee et al., 2022). ~~There are differences in the~~The applicability of ~~different RTM~~various rainfall threshold models and ~~different~~ regression methods ~~in different~~differs across regions (Marin, 2020; Segoni et al., 2018). Therefore, to ~~decrease~~reduce uncertainty in ~~LHW, several~~landslide hazard warnings, multiple regression methods and ~~RTM must~~rainfall threshold models should be ~~used~~employed to ~~establish~~determine the ~~best~~most appropriate ~~rainfall~~ threshold for a ~~certain~~specific location.

Given that many researchers have employed the log-log ~~coordinates~~coordinate system for ~~RTM~~ regression analysis of rainfall threshold models (He et al., 2020), this study proposes to use of the multilayer perceptron (MLP) regression method to ~~study the~~examine rainfall thresholds under various rainfall durations. ~~Simultaneously~~Additionally, the third~~-~~-dimension indicator~~ "~~, "daily rainfall~~ for the day~~" (R) was ~~introduced~~incorporated to ~~create~~develop the E-D-R ~~RTM based on~~rainfall threshold model, extending the E-D ~~RTM~~rainfall threshold model (Liu et al., 2022).

In this study, the Three Gorges Reservoir Area ~~(TGRA)~~ was ~~used~~selected as the study area~~, and the landslides~~. Landslides were ~~first~~ catalogued to ~~get~~obtain the E and D data ~~during~~for the five days ~~before the landslides~~preceding each landslide, as well as the R data at the time of the landslides. ~~Following that~~Subsequently, the rainfall thresholds corresponding to the E-D and E-D-R models for ~~distinct~~varying landslide occurrence probabilities were calculated using both OLS and MLP regression methods~~, respectively. To~~. The study aims to explore the optimal ~~RTM~~rainfall threshold model for the study area ~~and~~, assess the feasibility of neural ~~network for RTM research, as well as to~~ networks in rainfall threshold modeling, and categorize ~~RWL~~rainfall warning levels based on the optimal ~~RTM. Then, select the~~model. Landslide-inducing factors ~~that induce~~ were selected, and landslide ~~occurrence and predict the LS results~~susceptibility was predicted using RF, SVM, and 3D convolutional neural network (CNN-3D) models~~, and utilize the LS~~. The most accurate susceptibility results ~~with the best accuracy~~were used as the spatial probability of landslide occurrence in the study area. Finally, the daily ~~RWL is~~ rainfall warning level was combined with the ~~LS result~~ landslide susceptibility results using ~~the~~a superposition matrix to ~~achieve the~~generate daily ~~LHW, which serves as~~landslide hazard warnings, providing a reference for ~~precision~~the precise prevention and management of local landslide disasters. The study flowchart is shown in Fig. 1.

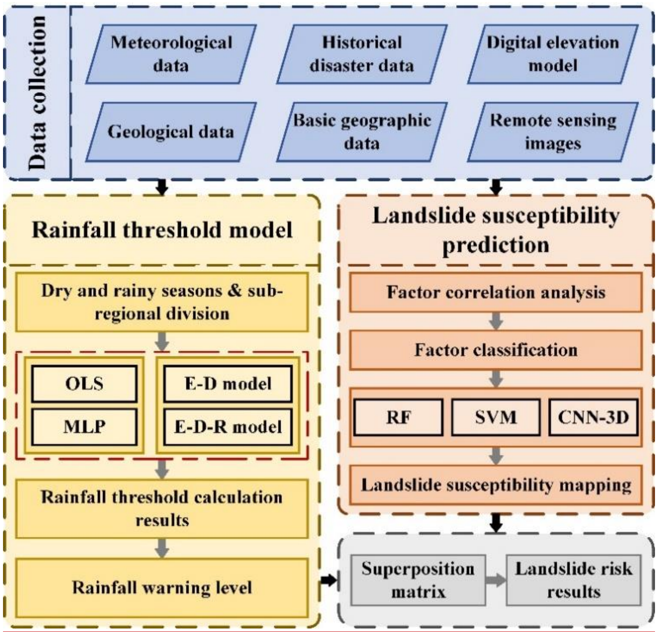

Figure 1. Flowchart of this study.

2. Methods

2.1 Rainfall Threshold Model

2.1.1 OLS Regression

OLS regression is a ~~commonly~~widely used linear regression ~~method that can be used to establish~~technique for establishing a linear relationship between ~~the~~an independent variable (x) and ~~the~~a dependent variable (y). It minimizes the ~~error~~difference between the predicted ~~value~~ and ~~the actual~~ observed value by ~~seeking~~finding the slope and intercept that best fits the data (Lim et al., 2023).

The basic form of ~~its~~the OLS regression model ~~can be~~is expressed as:

$$y = \beta_0 + \sum_{i=1}^{n} \beta_i x_i \, , \tag{1}$$

where y denotes the dependent variable, x_i denotes the independent variable, n denotes the number of independent variables, β_i denotes the coefficients of the independent variables, and β_0 denotes the constant intercept.

2.1.2 MLP Regression

MLP is a ~~common~~ commonly used neural network ~~with the ability~~capable of nonlinear mapping, ~~which can~~enabling it to learn complex nonlinear functional relationships through multiple layers of nodes. ~~Currently, it~~ It has been widely ~~used~~applied in ~~many~~various fields~~ such as~~, including geospatial analysis (Hasan et al., 2023; Wang et al., 2023b), aerodynamics (Barcenas et al., 2023), atmospheric science (Hoffman and Jasinski, 2023), rainfall prediction (Narimani et al., 2023), and image fusion (Mei et al., 2023). In ~~the~~ regression analysis of scatter data, a scatter data set ~~can be regarded~~is treated as ~~composed~~a collection of ~~multiple~~ input-output data pairs~~, and the~~. The model adjusts ~~the~~its weights ~~of the model~~ by minimizing the error between ~~the~~ predicted ~~value~~ and ~~the~~ actual data, ~~and finally realizes the~~ultimately achieving accurate regression~~ of scatter data. In this study, we built an MLP model with two hidden layers (Fig. 1).~~.

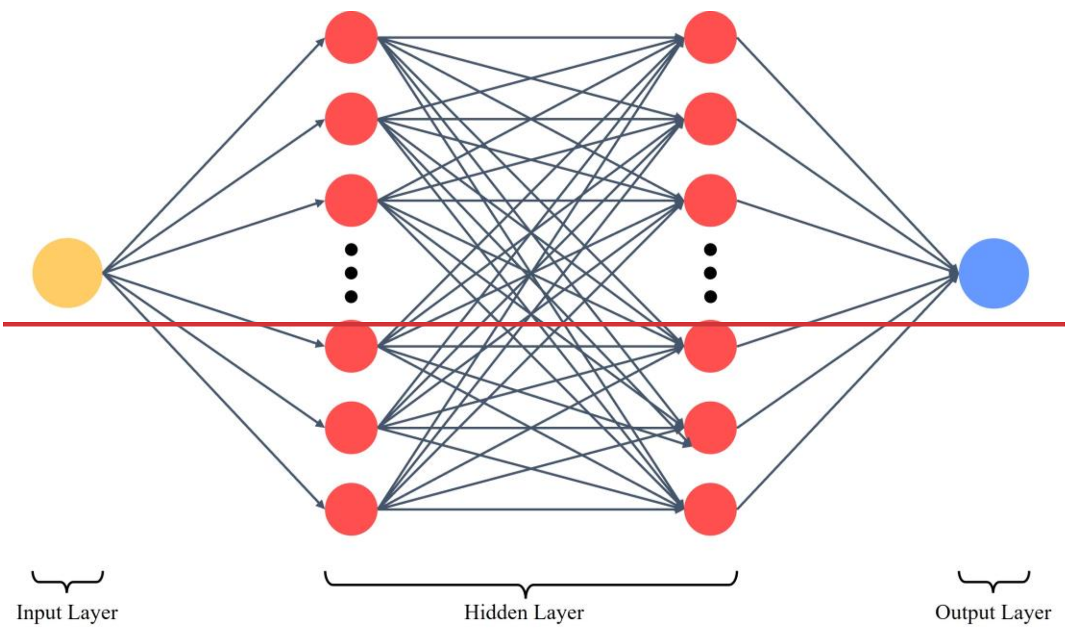

~~**Figure 1: Schematic diagram of the MLP model.**~~

2.1.3 E-D-R Rainfall Threshold Model

The E-D-R ~~RTM is based on~~rainfall threshold model builds upon the E-D ~~RTM, with the introduction of~~rainfall threshold model by introducing the R ~~metrics at the~~ metric as a third ~~latitude~~dimension to optimize the original ~~RTM~~model. To ~~investigate~~analyze the E-D-R ~~RTM,~~rainfall threshold model, it is essential first to establish the E-D ~~RTM must first be determined~~rainfall threshold model.

The E-D ~~RTM aims to investigate the~~rainfall threshold model examines the relationship between effective rainfall ~~as a function of~~and the duration of rainfall (Teja et al., 2019). The scatter plot is ~~generally~~typically analyzed ~~by~~using regression in a log-log ~~coordinates~~coordinate system, ~~and then~~with the resulting fitted ~~straight~~ line ~~is~~then transformed into a ~~result in a~~ Cartesian coordinate system. The expression for this is:

$$E = \alpha \times D^{\beta} , \tag{2}$$

Assume ~~that~~ the linear equation ~~obtained by fitting~~fitted in the log-log ~~coordinates~~coordinate system has an intercept of b and a slope of a. Then, in ~~the above equation~~this context, $\alpha = 10^{b}$, $\beta = a$, ~~and~~where D denotes the duration of rainfall (~~d).~~ in days), and E is the effective rainfall (in mm), ~~which refers to~~defined as the total ~~amount of~~ rainfall that ~~actually~~ infiltrates and ~~acts on~~impacts the landslide~~ body in addition to the~~, excluding slope runoff and evaporation (Huang et al., 2022a). The effective rainfall formula ~~used~~applied in this study is~~ as follows~~:

$$E = \sum_{i=1}^{n} k^{i-1} E_i , \tag{3}$$

where E denotes the effective rainfall, E_i is the rainfall on the previous i days, and k is the effective rainfall coefficient~~. The value of k is usually~~, typically set to 0.8 (Huang et al., 2022a). ~~Furthermore~~Additionally, it has been ~~shown~~demonstrated that ~~the~~ effective rainfall ~~in~~within the first 5 days ~~of the TGRA has a strong link~~in the Three Gorges Reservoir Area is strongly correlated with landslide events (Zhou et al., 2022). Therefore, the number of days ~~of~~n considered for rainfall statistics ~~n~~ in this ~~work~~study is set to 5.

The indicator R is introduced as a third dimension ~~of the indicator R is added based on~~to extend the E-D ~~RTM to expand the~~rainfall threshold model from two to three dimensions, ~~and the RTL meet~~resulting in a model that satisfies the following relational equation:

$$T = \max\{G_E, G_R\} , \tag{4}$$

where T denotes the final ~~RWL~~rainfall warning level, while G_E and G_R denote the ~~RWL~~rainfall warning levels for the E-D model and ~~R~~R dimension, respectively.

2.2 CNN-3D Model

A Convolutional Neural Network (CNN) is a deep learning algorithm~~, widely used~~ extensively utilized in image recognition (Fan et al., 2022; Gill et al., 2022), natural language processing (Jin et al., 2023; Kaliyar et al., 2021) and various other domains. ~~Its primary concept is to extract~~The core principle of CNN involves extracting features from input data ~~using a~~through convolution ~~operation~~operations (Youssef et al., 2022). However, ~~for~~in one- and two-dimensional CNNs, feature extraction for induced factor data is ~~only~~typically performed at a single raster point. Both methods ~~ignore~~overlook the spatial information ~~around~~surrounding the raster points (Yang et al., 2022). ~~As a result~~Consequently, this study ~~presents~~introduces CNN-3D ~~in order~~ to fully ~~use~~leverage the rich spatial information ~~around the~~surrounding raster points~~ in order to increase~~, thereby enhancing the prediction accuracy of ~~LS.~~landslide susceptibility. The structure of CNN-3D ~~is similar to~~mirrors that of traditional CNN, but ~~since the input~~due to the inclusion of additional spatial data~~ contains more information~~, CNN-3D can ~~provide~~yield more accurate results (Liu et al., 2023).

~~We picked a~~A three-dimensional structure was selected to ~~create~~generate samples in this experiment. ~~Before producing the samples~~Prior to sample generation, an n-channel ~~picture~~image is ~~formed~~created by superimposing ~~n~~n components. Each pixel is then extended ~~outwards~~outward by 7 pixels~~ to generate ~~, resulting in a 15 × 15 × ~~n~~n image used as input. Subsequently, ~~through ~~operations such as convolution and pooling in the hidden layer~~, the~~ map high-level features ~~are mapped ~~to ~~the~~a low-dimensional space~~ and~~, which are then stored in the neural units of the fully connected layer~~, and finally classified~~. Finally, classification is performed using the Softmax function to ~~obtain the results of landslides~~determine landslide and non-~~slides (Fig. 2).~~

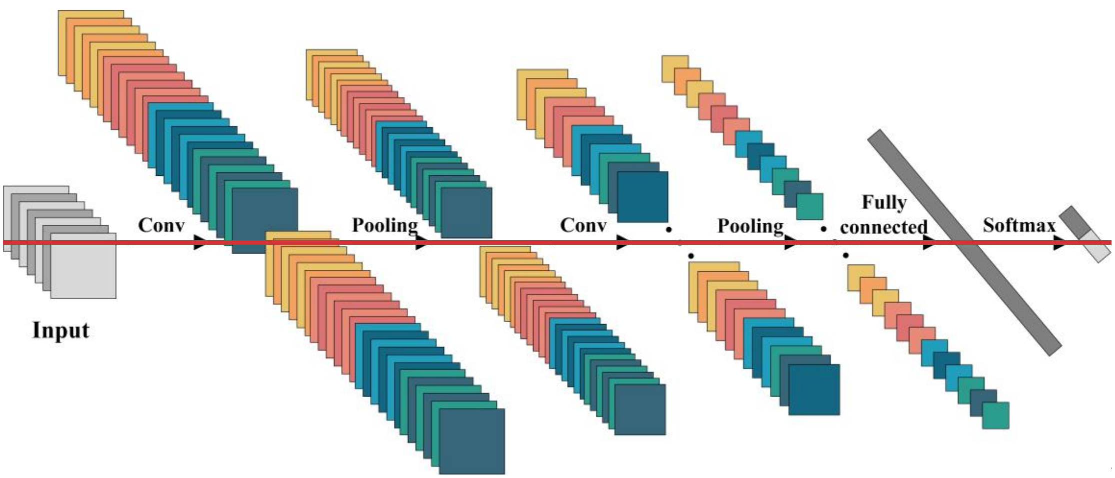

~~Figure 2: Schematic diagram of CNN-3D structure~~landslide outcomes.

3. Overview of the Study Area

3.1 Physical and Geographical Characteristics

The study area is located in the upper reaches of the Yangtze River~~ between ~~, extending from Sandouping in Yichang City ~~and~~to Jiangjin District in Chongqing~~, which is situated at longitude~~. It lies between longitudes 105°50′~~-~~E and 111°42′~~-~~E and ~~latitude~~latitudes 28°30′~~-~~N and 31°45′~~–~~N (Cheng et al., 2022)~~, encompassing a total of ~~. This area encompasses 29 administrative districts and counties, including 7 in Hubei Province and 22 in Chongqing Municipality~~ (7 districts and counties in Hubei, and 22 districts and counties in Chongqing), and~~, covering a total area of 5.67×10^4 km^2 (Fig. ~~3~~2).The ~~climate of the ~~region ~~is~~experiences a subtropical monsoon climate, with ~~an ~~average annual precipitation ~~of~~ranging from 445~~-~~ to 1813 mm (Long et al., 2021). ~~And the~~The abundant rainfall in the ~~area~~region is a ~~major~~significant factor ~~inducing landslides~~contributing to landslide occurrences (Guo et al., 2022).

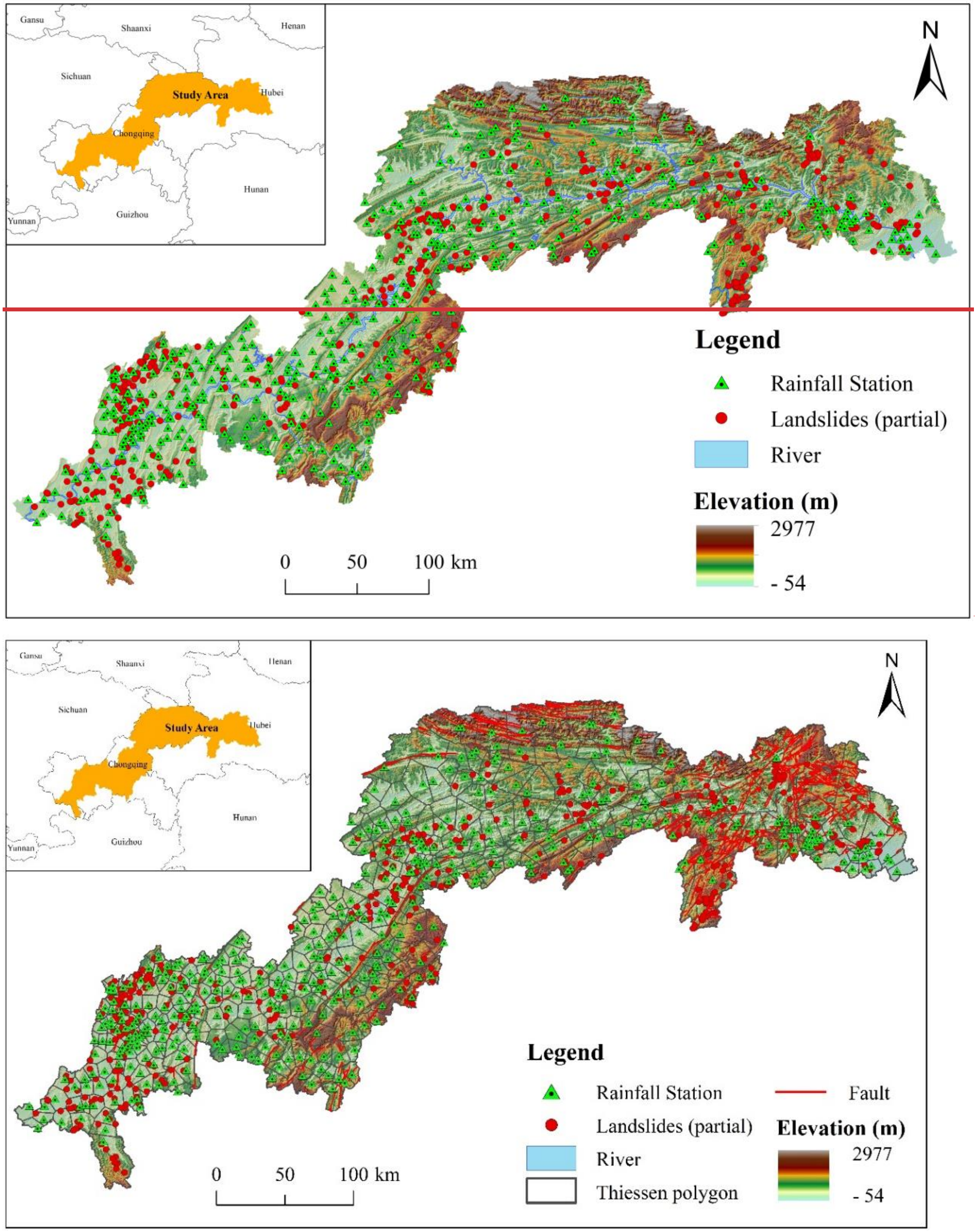

Figure ~~3~~2: Geographic location of the study area and Thiessen polygon results for rainfall stations.

3.2 Landslide Data Cataloguing~~Geomorphology, geology,~~ and Study Area Subdivision

Cataloging landslide data is crucial for studying rainfall thresholds (Gariano et al., 2021). This process involves recording essential information, including the time of occurrence, geographic location, and associated rainfall stations for each landslide event. The historical landslide data used in this study were provided by the Wuhan Geological Survey Center (http://www.wuhan.cgs.gov.cn/). To identify the corresponding rainfall stations for each historical landslide, the Thiessen polygon method was employed to match each landslide point with the nearest rainfall station (Zhao et al., 2019), thereby obtaining the pre-landslide rainfall data (see Fig. 2, Thiessen polygons).

After filtering and cleaning, a total of 453 historical landslides with accurate rainfall information, dates, and locations were identified (see Fig. 2, Landslides). Historical rainfall data indicate that precipitation in the study area is primarily concentrated between May and October. The differing climatic conditions between the dry and rainy seasons may lead to varying impacts of rainfall on landslide movements (Soralump et al., 2021). ~~climate play the most important role in preparatory process of landslide initiation in any region~~Based on this information, the historical landslides were classified into rainy season and dry season landslides according to their occurrence times (Fig. 3(b)).

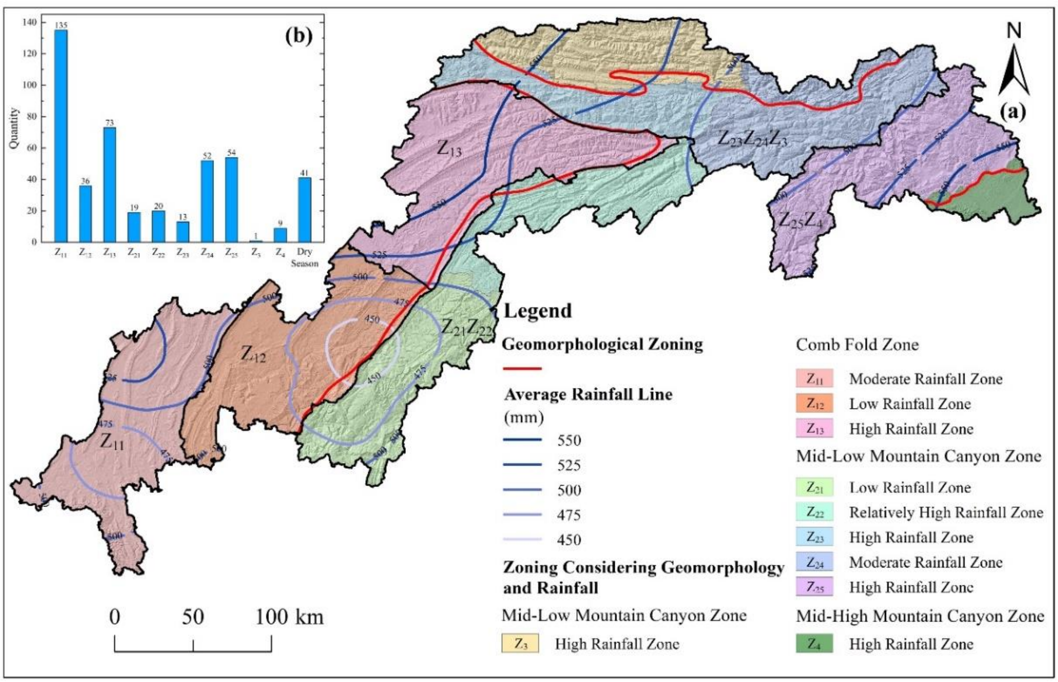

Figure 3: Zoning map of the study area. (a) Schematic diagram of the sub-region merger; (b) Number of historical landslide hazard sites in each sub-region.

Given the substantial influence of geomorphological, geological, and climatic conditions on landslide triggers during the rainy season (Dahal and Hasegawa, 2008), ~~and the differences between them lead to different~~ rainfall thresholds ~~in various~~

can vary across different regions. ~~Therefore, in~~ Accordingly, this study~~,~~ further subdivided the landslide data from the ~~whole~~rainy season. The study area was divided into ~~10 zones (Fig. 4) by considering the topography~~several sub-regions based on terrain and climatic conditions ~~of the study area, and the optimal RTM was~~, with rainfall thresholds calculated for each ~~zone separately. Among them, Z_{11}, Z_{12} and Z_{13} are the moderate rainfall zone, low rainfall zone and high rainfall zone in the folded~~ region~~;~~. However, due to the limited historical landslide data in regions Z_{21}, Z_{22}, Z_{23}, ~~Z_{24}~~Z_3 and Z_4, adjacent regions were merged to mitigate potential inaccuracies in rainfall threshold calculations caused by insufficient data. Specifically, Z_{21} and Z_{22} were combined; Z_{23}, Z_{24}, and Z_3 were combined; and Z_{25} ~~are the low rainfall zone,~~and Z_4 were combined. The final regional subdivision is illustrated in Fig. 3(a). For dry season landslides, due to relatively ~~high~~uniform rainfall ~~zone, high rainfall zone, moderate rainfall zone~~ and ~~high rainfall zone in the low and medium mountain region, respectively; Z_3 is the high rainfall zone in the medium and high mountain region; and Z_4 is the high rainfall zone in the hilly and plain zone~~the small number of events, no further subdivision was performed, and the rainfall threshold was calculated for the entire study area.

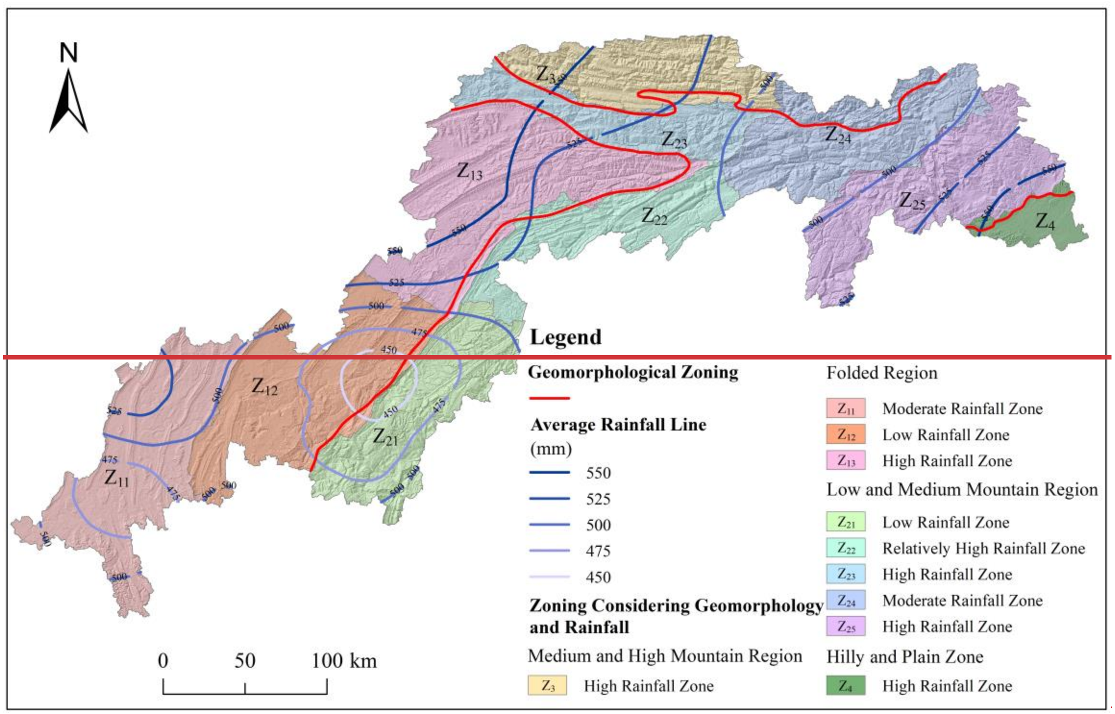

~~**Figure 4: Zoning map of the study area.**~~

~~Before landslide data cataloguing, the corresponding rainfall dataset needs to be acquired. Based on the abundance of rainfall stations in the study area (refer to Fig. 3, Rainfall Station), Thiessen polygon method were used for the delineation (Zhao et al., 2019), which facilitates the finding of rainfall stations corresponding to landslides. The Thiessen polygon method results satisfy the following conditions: (1) each polygon contains one and only one rainfall station; (2) any point within each~~

~~polygon is the closest to the rainfall station within the unit; (3) the points on the boundary are the same distance to the two neighboring rainfall stations. The result of its division is shown in Fig. 5.~~

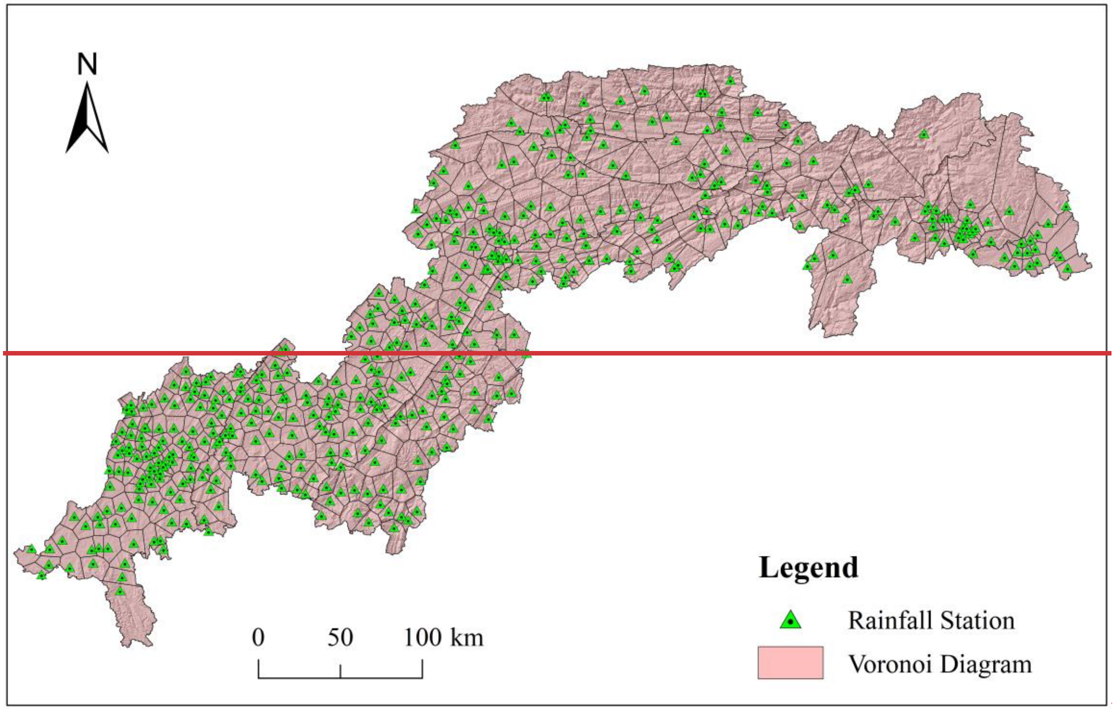

~~**Figure 5: Thiessen polygon method results map.**~~

~~Landslide data cataloguing is the basis for the study of rainfall thresholds (Gariano et al., 2021), and its main contents include basic information such as the time of occurrence of landslides, geographic location, associated rainfall stations, and so on. The landslide cataloguing data in this study were obtained from the historical landslide hazard data provided by Wuhan Geological Survey Centre (http://www.wuhan.cgs.gov.cn/).~~

~~A total of 453 historical landslides with precise rainfall information, particular dates, and places were acquired by aggregating historical landslide data, removing landslides with no rainfall and missing rainfall data (refer to Fig. 3, Landslide).~~

~~The rainfall in the study area is mainly concentrated from May to October, and the differences in climatic conditions between the dry and wet seasons might result in various impacts of rainfall on landslide movement (Soralump et al., 2021). Therefore, in this study, according to the time of occurrence of historical landslides, landslides occurring from May to October are classified as rainy season landslides, while landslides occurring from November to April are classified as dry season landslides. According to the records, there were 412 rainy season landslides and 41 dry season landslides (Fig. 6). Among them, rainfall thresholds for rainy season landslides were calculated separately according to the sub-districts;~~

~~whereas the number of dry season landslides is small and further subdivision is not conducive to the calculation of rainfall thresholds, so only rainfall thresholds for dry season landslides were calculated for the entire study area.~~

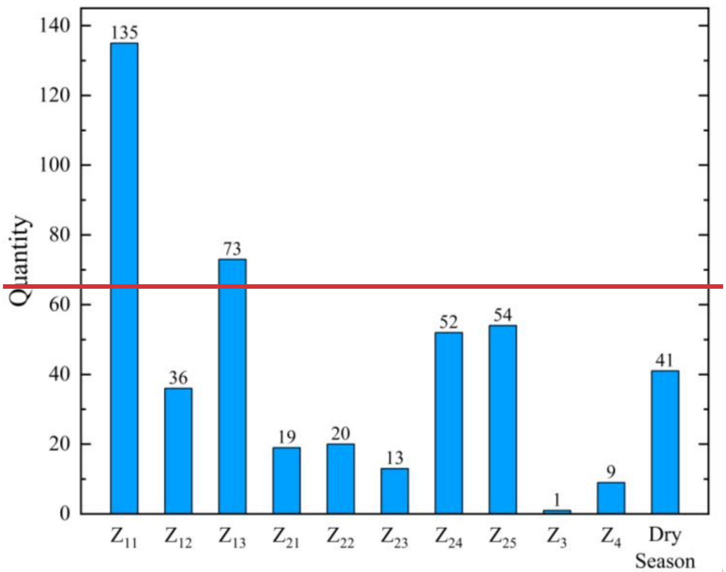

~~**Figure 6: Number of landslides in each sub-district in the rainy season and the whole region in the dry season.**~~

~~Figure 6 shows that the five zones Z_{21}, Z_{22}, Z_{23}, Z_3 and Z_4 have less catastrophe spots. To avoid insufficient data affecting rainfall threshold accuracy, this study merged some neighboring regions (Z_{21} and Z_{22} merged; Z_{23}, Z_{24}, and Z_3 merged; and Z_{25} and Z_4 merged) based on the geographic location of each region for rainfall threshold calculation.~~

4. Results

4.1 Rainfall Threshold Model Results

4.1.1 E-D Rainfall Threshold Model

Rainfall-triggered ~~landslide is a random~~landslides are rare and ~~small probability event, and if only~~probabilistic events. Relying solely on the minimum threshold ~~is used to warn of~~for geological hazards~~, it will produce many~~ warnings can result in numerous ineffective warnings (i.e., False Positive Error) (Sarkar et al., 2023). ~~While decreasing the public's~~This not only diminishes public trust in disaster warning, ~~it will result in a waste of~~but also leads to wasted resources ~~for~~on preventive and control activities, ~~which is not favorable to the advancement of~~ impeding progress in disaster prevention and mitigation. ~~Therefore~~Consequently, most ~~of the~~ current studies on ~~RTM use a variety of~~rainfall threshold models utilize various threshold curves with different landslide probabilities (Sheng et al., 2022), ~~in order~~ to ~~improve~~enhance the ~~reasonableness~~reliability and accuracy of rainfall ~~warning. Generally, the~~warnings. Typically, landslide probability

~~indicates~~refers to the proportion of ~~the number of~~ landslides triggered by rainfall exceeding a ~~certain~~specified threshold ~~among all occurring~~relative to the total number of landslides (Yang et al., 2020).

~~In the calculation of~~For OLS regression calculation, the E and D ~~scatters of~~data from historical landslide hazard locations ~~in each area~~ were ~~first~~initially plotted ~~into~~in the E-D log-log ~~coordinates~~coordinate system~~, and the~~. The 50% landslide probability rainfall threshold curve was then derived by fitting this data using OLS regression. The fitted curves were ~~then used~~subsequently employed to ~~run~~perform OLS regression analysis on ~~the~~ historical landslide hazard points above and below ~~the~~these curves~~ to get~~, resulting in the 75% ~~landslide probability rainfall threshold curve and the~~and 25% landslide probability rainfall threshold ~~curve~~curves (Fig. ~~7~~4). Finally, the straight lines from the log-log ~~coordinates~~coordinate system ~~straight lines~~ were ~~transformed to~~ converted into curves in the Cartesian coordinate system ~~curves~~ (Table 1).

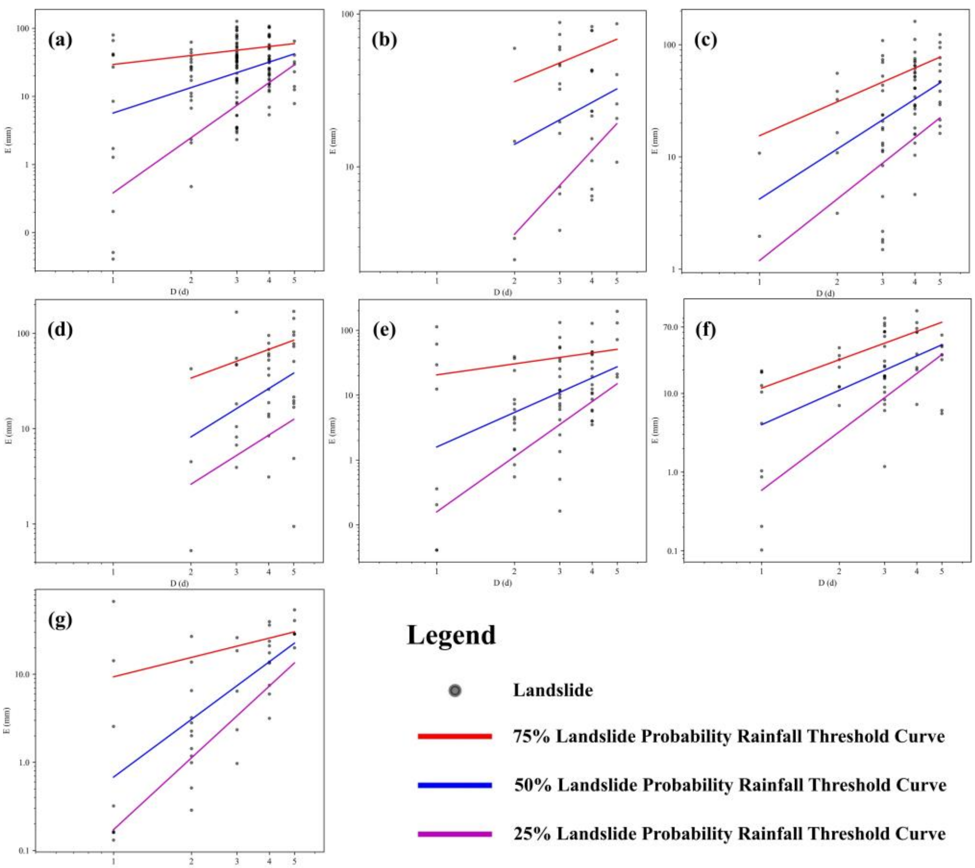

Figure ~~7: Plot of~~4: E-D rainfall threshold model results plotted in the log-log ~~coordinates~~coordinate system ~~(~~using OLS regression~~)~~. In the figure, regions are labelled as follows: a ~~is~~represents the Z_{11} region, b ~~is~~represents the Z_{12} region, c ~~is~~represents the Z_{13} region, d ~~is~~represents the $Z_{21}Z_{22}$ region, e ~~is~~represents the $Z_{23}Z_{24}Z_{3}$ region, f ~~is~~represents the $Z_{25}Z_{4}$ region, and g ~~is~~represents the Dry Season.

Table 1: E-D rainfall threshold equation ~~(~~derived from OLS regression~~)~~.

Region	Landslide probability	Equations (Log-log coordinates system)	E-D equation
Z_{11}	75%	y=0.4383x+1.4679	$E=29.3697\times D^{0.4383}$
	50%	y=1.2420x+0.7552	$E=5.6912\times D^{1.2420}$
	25%	y=2.6894x-0.4164	$E=0.3834\times D^{2.6894}$
Z_{12}	75%	y=0.6981x+1.3464	$E=22.2024\times D^{0.6981}$
	50%	y=0.9113x+0.8721	$E=7.4490\times D^{0.9113}$
	25%	y=1.8193x+0.0102	$E=1.0238\times D^{1.8193}$
Z_{13}	75%	y=1.0019x+1.1887	$E=15.4419\times D^{1.0019}$
	50%	y=1.4792x+0.6246	$E=4.2131\times D^{1.4792}$
	25%	y=1.8201x+0.0759	$E=1.1910\times D^{1.8201}$
$Z_{21}Z_{22}$	75%	y=0.9977x+1.2307	$E=17.0098\times D^{0.9977}$
	50%	y=1.6825x+0.4075	$E=2.5556\times D^{1.6825}$
	25%	y=1.7100x-0.0969	$E=0.8000\times D^{1.7100}$
$Z_{23}Z_{24}Z_{3}$	75%	y=0.5633x+1.3125	$E=20.5353\times D^{0.5633}$
	50%	y=1.7673x+0.2014	$E=1.5900\times D^{1.7673}$
	25%	y=2.8230x-0.7986	$E=0.1590\times D^{2.8230}$
$Z_{25}Z_{4}$	75%	y=1.1974x+1.0675	$E=11.6815\times D^{1.1974}$
	50%	y=1.4525x+0.6027	$E=4.0059\times D^{1.4525}$
	25%	y=2.4652x-0.2305	$E=0.5882\times D^{2.4652}$
Dry Season	75%	y=0.7295x+0.9706	$E=9.3454\times D^{0.7295}$
	50%	y=2.1754x-0.1679	$E=0.6794\times D^{2.1754}$
	25%	y=2.7079x-0.7646	$E=0.1719\times D^{2.7079}$

In the ~~calculation of~~ MLP regression analysis, the rainfall thresholds ~~corresponding to~~for a 50% landslide probability were initially fitted separately for each duration of rainfall (D~~) were first fitted separately. The~~). MLP regression was then ~~performed on the~~ applied to historical landslide data above and below ~~the~~these thresholds~~, respectively,~~ to ~~obtain the 75% landslide probability and 25% landslide probability~~ determine the rainfall thresholds ~~corresponding to~~for 75% and 25% landslide probabilities for each D. ~~Due to the lack of~~Limited historical landslide ~~hazard~~ data ~~at~~for a D of 1 in some regions (e.g., ~~region~~ Z_{12}) and ~~the small amount of historical landslide hazard~~insufficient data ~~at~~for a D of 5 in ~~some~~other regions (e.g., ~~region~~ Z_{11}~~), these can~~) may lead to ~~irrational results of~~inaccuracies in the fitted rainfall thresholds. ~~In~~To address this ~~regard, this study used~~issue, Gaussian regression (Kumar and Kavitha, 2021) and GM(1,1) grey prediction model (Chen and Huang, 2013) were employed to correct the rainfall ~~threshold results obtained~~thresholds derived from MLP regression. The corrected results are shown in Fig. ~~8~~5 and Table 2.

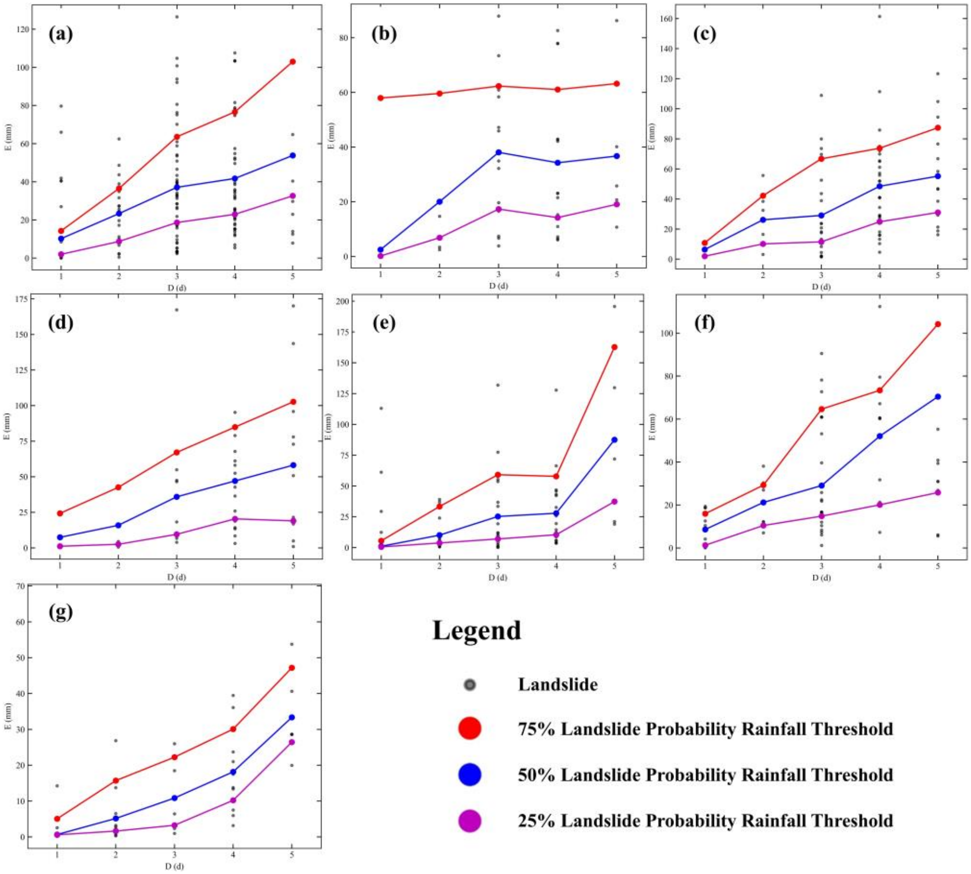

Figure ~~8: Plot of~~5: E-D rainfall threshold model results ~~(~~plotted using MLP regression~~)~~. In the figure, regions are labelled as follows: a ~~is~~represents the Z_{11} region, b ~~is~~represents the Z_{12} region, c ~~is~~represents the Z_{13} region, d ~~is~~represents the $Z_{21}Z_{22}$ region, e ~~is~~represents the $Z_{23}Z_{24}Z_3$ region, f ~~is~~represents the $Z_{25}Z_4$ region, and g ~~is~~represents the Dry Season. The red, blue, and purple points ~~in Fig. 8 are the~~denote rainfall threshold ~~points obtained from the fit~~values fitted for ~~different~~various landslide probabilities. ~~The line~~Line segments are ~~just~~included solely for ~~connecting the individual threshold points for viewing purposes~~visual clarity and ~~have no~~ do not convey any practical information.

Table 2: E-D rainfall threshold ~~(~~derived from MLP regression~~)~~.

Region	Duration of rainfall (D)	75% threshold (mm)	50% threshold (mm)	25% threshold (mm)
	1	14.2305	10.1800	1.9625
	2	36.4914	23.3267	8.7024
Z_{11}	3	63.5907	37.0893	18.6210
	4	76.6291	41.7210	22.9260
	5	103.0000	53.8090	32.6260
	1	57.9690	2.4749	0.1550
Z_{12}	2	59.6126	20.0312	6.8458
	3	62.3002	38.0666	17.3107
	4	61.0451	34.2639	14.1966

	5	63.2107	36.7170	19.0748
	1	10.8122	6.3897	1.9677
	2	42.1870	26.1761	10.1656
Z_{13}	3	66.7259	29.0723	11.5028
	4	73.7542	48.4590	24.8502
	5	87.3909	55.1944	31.0476
	1	24.2575	7.4117	1.1585
	2	42.5658	15.8642	2.5160
$Z_{21}Z_{22}$	3	67.0825	35.8785	9.5152
	4	84.8807	47.0166	20.3769
	5	102.6789	58.1546	18.9942
	1	5.5210	1.0893	0.5702
	2	33.3538	10.1252	3.7901
$Z_{23}Z_{24}Z_3$	3	59.1386	25.2715	7.0353
	4	57.8357	27.9044	10.4444
	5	162.7467	87.5204	37.3694
	1	15.9482	8.6114	1.2742
	2	29.2418	21.1900	10.4545
$Z_{25}Z_4$	3	64.6284	29.0526	14.8209
	4	73.3920	52.0651	20.0756
	5	104.1990	70.4430	25.8100
	1	5.0503	0.6647	0.5818
	2	15.7035	5.1495	1.6332
Dry Season	3	22.2420	10.8428	3.2452
	4	30.0733	18.1523	10.2084
	5	47.1948	33.3588	26.4428

The threshold curves ~~generated~~derived from OLS regression in the log-log ~~coordinates~~coordinate system ~~often exhibit~~typically display an upward trend, as ~~shown~~illustrated in Fig. ~~7, and~~4, with the slopes of the rainfall threshold curves for 25%, 50%, and 75% landslide ~~probability gradually decrease. From Fig. 8~~probabilities decreasing progressively. As shown in Fig. 5, the rainfall thresholds obtained from MLP regression for ~~different~~various landslide probabilities ~~also show a~~ generally exhibit an increasing trend~~, but~~. However, the ~~relatively small amount of~~limited historical landslide data in some subregions ~~results in relatively unreasonable~~leads to less accurate rainfall thresholds (e.g., the rainfall threshold for the $Z_{23}Z_{24}Z_3$ region shows a large increase when D is 5).

4.1.2 E-D-R Rainfall Threshold Model

~~Based~~Building on the ~~above~~ E-D rainfall threshold model, the third dimension indicator R was ~~introduced~~incorporated to ~~construct~~develop the E-D-R rainfall threshold model. In this model, the value of R is ~~taken equal~~set to the rainfall threshold corresponding to ~~when~~ a duration of D ~~is~~equal to 1 in the E-D ~~RTM.~~rainfall threshold model. These three indicators

~~visually~~collectively form a closed "box" (Fig. ~~9), with~~6), demonstrating "nested" relationships ~~between the~~among different landslide probability levels.

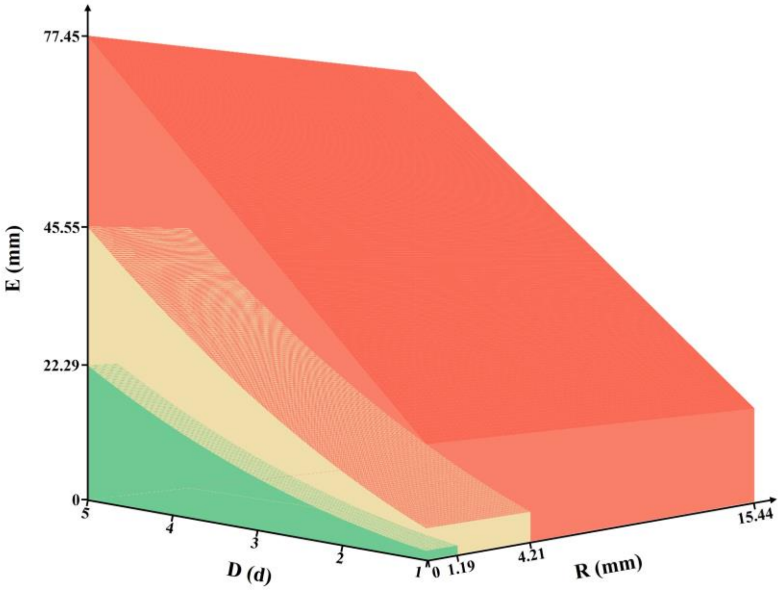

Figure ~~9~~6: Schematic diagram of the E-D-R rainfall threshold model ~~obtained from~~illustrated using the OLS regression ~~(~~results from the Z13~~).In Fig. 9, the~~ region as an example. The green, yellow, and red boxes ~~indicate~~in the figure represent landslide probabilities corresponding to rainfall thresholds of <25%, 25-50%, and 50-75%, respectively.

4.1.3 Model Accuracy Verification

The accuracy of the model was ~~tested in this research utilizing~~evaluated using 82 landslide ~~hazards~~hazard events from 2019 and 2020 that were not ~~involved~~included in the ~~RTM~~ rainfall threshold model calculations~~ in 2019 and 2020.~~. Figure ~~10 depicts~~7 shows the ~~number~~distribution of landslide ~~hazards~~hazard events ~~in each region~~across different regions.

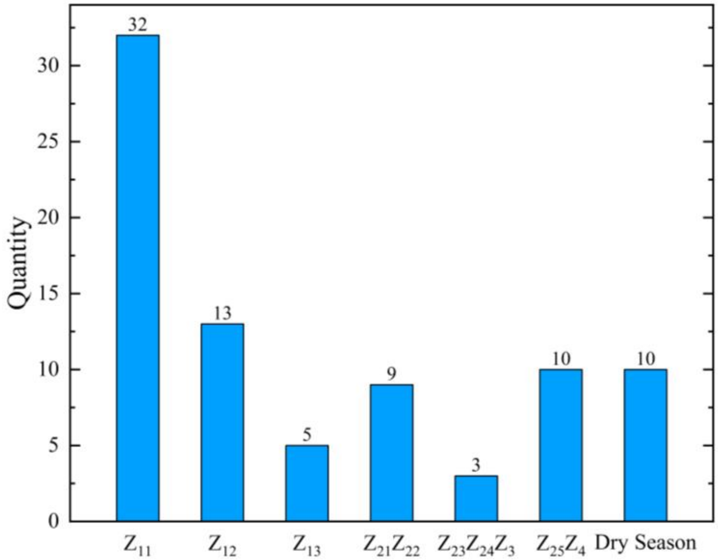

Figure ~~10: The number~~7: Number of landslide hazard events in each region of the validation set.

In ~~the actual~~practical landslide ~~control work, it is impossible to obtain the~~prevention, real~~-rainfall on a certain day in the~~ -time future~~, so it can only be replaced by the forecast~~ rainfall~~. In order to make the~~ data is unavailable and must be substituted with forecasted rainfall. To enhance the realism of the validation data ~~source of~~for the rainfall threshold model ~~more realistic~~, this study ~~relies on the abundant~~used numerous rainfall ~~forecasting~~forecast stations ~~in~~within the study area ~~(Fig. 11) and counts the forecast~~to gather forecasted rainfall amounts for the 82 landslide events on the day of ~~the~~ occurrence ~~of these 82 landslide hazards as well as the previous 5~~and for the five days ~~for~~prior. Notably, the ~~validation of the model. The~~ rainfall forecast stations ~~in Fig. 11 are distributed~~used here were established later and differ from the rainfall stations used in the landslide cataloguing (Fig. 2, Rainfall Station). These forecast stations, covering the entire study area at 0.05° intervals, ~~and the forecast rainfall data were provided by the Wuhan Geological Survey Centre. The data are updated in~~provide real~~-time according to meteorological changes, and the data used in the study are adopted from the latest update of the forecast data to ensure the accuracy of the data~~-time updates on forecasted rainfall.

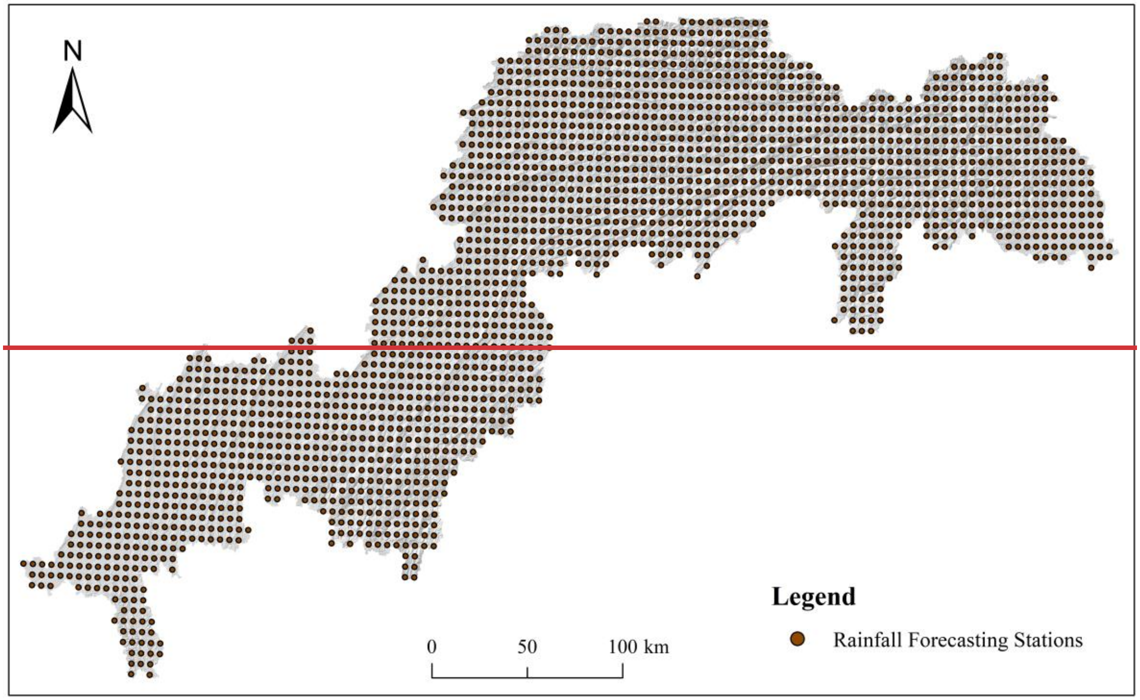

~~**Figure 11: Map of rainfall forecasting stations.**~~

The ~~research region~~study area was classified into four warning categories based on the rainfall threshold ~~classification~~ results: ~~attention~~Attention (<25%), ~~special attention~~Special Attention (25-50%), ~~warning~~Warning (50~~% -~~-75%), and ~~severe warning~~Severe Warning (≥75%). Figure ~~12 displays~~8 presents the ~~ultimate outcomes~~results of the validation process for each region's ~~four RTM~~rainfall threshold model categories. ~~Furthermore~~Additionally, Table 3 ~~displays~~shows the proportion of hazardous ~~circumstances~~situations corresponding to the ~~two warning~~“Severe Warning” and “Warning” levels ~~of “severe warning” and “warning”~~ in the E-D-R ~~RTM~~rainfall threshold model validation results.

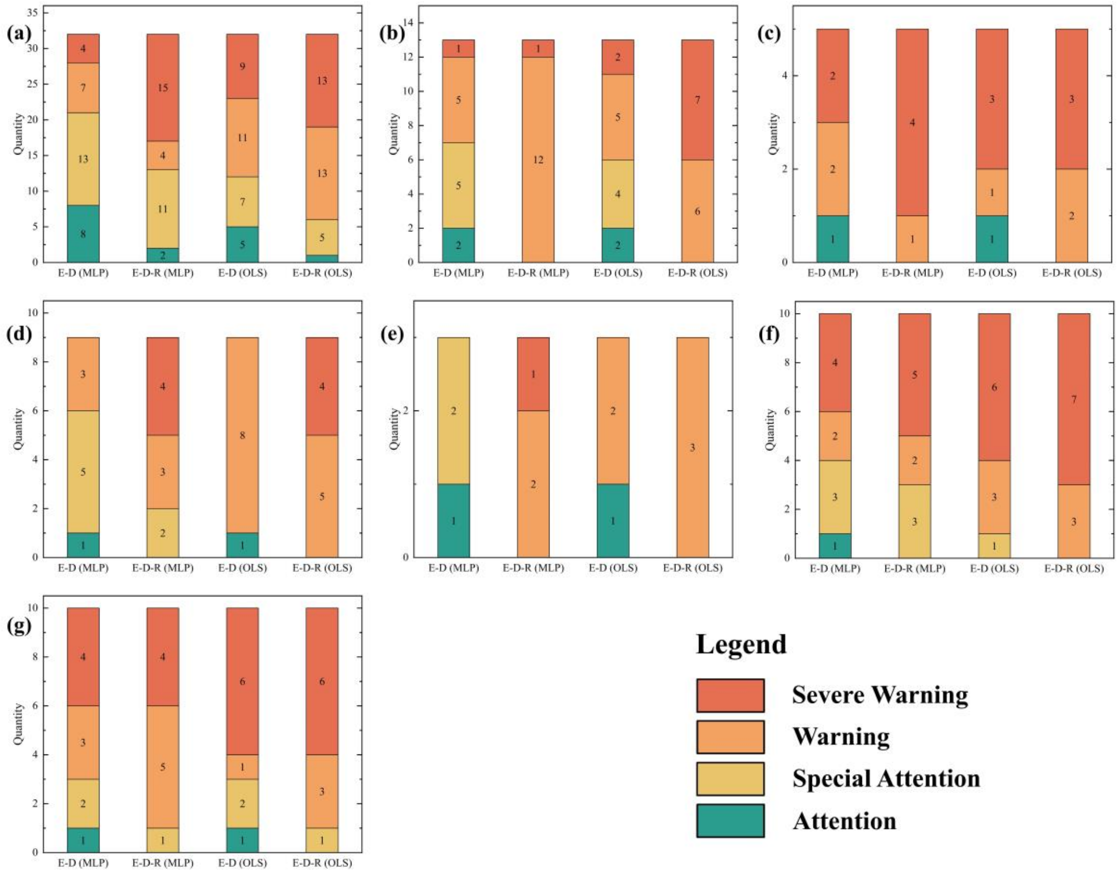

Figure ~~12: The distribution~~8: Distribution of warning levels in the validation set for each partitioned region. ~~In the figure, a is~~Regions are labelled as follows: a represents the Z_{11} region, b ~~is~~represents the Z_{12} region, c ~~is~~represents the Z_{13} region, d ~~is~~represents the $Z_{21}Z_{22}$ region, e ~~is~~represents the $Z_{23}Z_{24}Z_3$ region, f ~~is~~represents the $Z_{25}Z_4$ region, and g ~~is~~represents the Dry Season.

Table 3: Proportion of hazard events corresponding to the "Severe Warning" and "Warning" levels in the E-D-R ~~RTM~~rainfall threshold model for each partitioned region.

Region	Regression approach	Level	Percentage (%)
Z_{11}	MLP	Severe Warning	46.88
		Warning	12.50
	OLS	Severe Warning	40.63
		Warning	40.63
Z_{12}	MLP	Severe Warning	7.69
		Warning	92.31
	OLS	Severe Warning	53.85
		Warning	46.15
Z_{13}	MLP	Severe Warning	80.00
		Warning	20.00
	OLS	Severe Warning	60.00

		Warning	40.00
$Z_{21}Z_{22}$	MLP	Severe Warning	44.44
		Warning	33.33
	OLS	Severe Warning	44.44
		Warning	55.56
$Z_{23}Z_{24}Z_{3}$	MLP	Severe Warning	33.33
		Warning	66.67
	OLS	Severe Warning	0.00
		Warning	100.00
$Z_{25}Z_{4}$	MLP	Severe Warning	50.00
		Warning	20.00
	OLS	Severe Warning	70.00
		Warning	30.00
Dry Season	MLP	Severe Warning	40.00
		Warning	50.00
	OLS	Severe Warning	60.00
		Warning	30.00

The following conclusions ~~may~~can be drawn from ~~an analysis of~~analyzing the prediction accuracy of the four categories of ~~RTM:~~ rainfall threshold models:

(1) The ~~accuracies~~accuracy of the E-D-R ~~RTM~~ rainfall threshold model, as computed using both MLP regression and OLS regression~~ are much better than~~ , significantly surpasses that of the comparable E-D ~~RTM. The E-D-R RTM predict outputs~~rainfall threshold model. With the inclusion of the R indicator in the third dimension, the E-D-R rainfall threshold model's predictions no longer include the "Attention" warning level for all areas (except Z_{11} ~~excepted) when the R indicator was included in the third dimension. Furthermore~~). Moreover, there has been ~~a rise~~an increase in the percentage of hazard incidents ~~categorized as~~classified under the "Warning" and "Severe Warning" categories across all regions. Compared ~~with~~to the E-D model, the proportion of hazardous conditions categorized as "Warning" and "Severe Warning" in the ~~"Warning" and "Severe Warning" warning levels of the E-D-R RTM increases~~E-D-R rainfall threshold model increased from 41.46% to 76.82%, ~~and~~while the ~~result of~~proportion for OLS regression ~~increases~~rose from 69.51% to 91.46%.

(2) ~~The~~Although the prediction accuracies of the E-D-R ~~RTM for each region are~~rainfall threshold model vary slightly ~~different~~ between ~~the~~ MLP regression and ~~the~~ OLS regression~~, but in general~~ for each region, the ~~total~~overall proportion of hazardous conditions ~~at~~in the ~~warning levels of~~ "Warning" and "Severe Warning" ~~is~~levels remains similar.

~~(3) The optimal RTM for each region is shown in Table 4.~~

(3) Table 4 presents the optimal rainfall threshold model for each region. The E-D-R models obtained from MLP regression are identified as the optimal models for the Z_{13} and $Z_{23}Z_{24}Z_3$ regions, demonstrating the feasibility of utilizing neural networks (MLP) for rainfall threshold model research.

Table 4: Optimal ~~RTM~~rainfall threshold model for each partitioned region.

Region	Optimal rainfall threshold modelling (regression approach)
Z_{11}	E-D-R (OLS)
Z_{12}	E-D-R (OLS)
Z_{13}	E-D-R (MLP)
$Z_{21}Z_{22}$	E-D-R (OLS)
$Z_{23}Z_{24}Z_3$	E-D-R (MLP)
$Z_{25}Z_4$	E-D-R (OLS)
Dry Season	E-D-R (OLS)

~~The optimal RTM for Z_{13} and $Z_{23}Z_{24}Z_3$ regions are the E-D-R models obtained from the MLP regression, proving the feasibility of using neural networks (MLP) for RTM research.~~

4.2 Landslide Susceptibility Results

4.2.1 Landslide Inducing Factor Selection

~~Combined with~~Based on the research ~~results~~findings of previous scholars (Chen et al., 2021; Chen et al., 2020; Habumugisha et al., 2022; Li et al., 2022; Li et al., 2020; Rohan et al., 2023) and considering the ~~actual situation~~specific conditions of the study area, this study selected a total of 11 ~~landslide inducing~~ factors~~, including~~ that potentially induce landslides. These factors include elevation, Normalized Difference Vegetation Index (NDVI), Topographic Wetness Index (TWI), road density, stratigraphic lithology, tectonic density, river distance, slope, curvature, land cover, and slope structure~~, were selected in this study.~~ (Table 5).

Table 5: Sources of data for landslide-inducing factors.

Factor Category	Data Source	Inducing Factor
Topography and Geomorphology	Geological Map STRM DEM ~~(30m)~~	Elevation Slope Curvature Slope Structure
Geological Lithology	Geological Map	Stratigraphic Lithology Tectonic Density
Hydrological Factor	National Basic Geographic Database STRM DEM ~~(30m)~~	TWI River Distance
Land Use	Landsat Remote Sensing Image ~~(30m)~~	NDVI

		Land Cover Type
Human Engineering Activities	OpenStreetMap	Road Density

Among ~~them, the~~these factors, slope structure ~~considers~~refers to the relationship between the slope aspect of the ~~slope and the~~ inclination of the rock formation (Niu et al., 2014)~~, and different~~. Different types of slope structures can ~~lead to differences~~result in variations in landslide size and intensity. Based on ~~different~~the slope gradient (σ), slope direction (γ), and inclination (α) and tendency (β) of the rock formation, ~~the following eight types of~~ slope structures are classified into the following eight types (Table 6).

Table 6: Classification of slope structure types and ~~percentage of each type in~~their respective percentages within the study area.

~~Code~~Class	Relationship between α, β, γ and σ	Area (%)
~~A~~Nearly horizontal slope	$\alpha \le 5°$	1.720
~~B~~Over-dip slope	$\alpha > 5°$, $\lvert\gamma-\beta\rvert \in [0°, 30°)$ or $\lvert\gamma-\beta\rvert \in [330°, 360°)$, $\sigma > \alpha$	5.127
~~C~~Flat-dip slope	$\alpha > 5°$, $\lvert\gamma-\beta\rvert \in [0°, 30°)$ or $\lvert\gamma-\beta\rvert \in [330°, 360°)$, $\sigma = \alpha$	0.000
~~D~~Under-dip slope	$\alpha > 5°$, $\lvert\gamma-\beta\rvert \in [0°, 30°)$ or $\lvert\gamma-\beta\rvert \in [330°, 360°)$, $\sigma < \alpha$	13.581
~~E~~Dip-oblique slope	$\alpha > 5°$, $\lvert\gamma-\beta\rvert \in [30°, 60°)$ or $\lvert\gamma-\beta\rvert \in [300°, 330°)$	17.559
~~F~~Transverse slope	$\alpha > 5°$, $\lvert\gamma-\beta\rvert \in 60°, 120°)$ or $\lvert\gamma-\beta\rvert \in [240°, 300°)$	32.066
~~G~~Anticlinal-oblique slope	$\alpha > 5°$, $\lvert\gamma-\beta\rvert \in [120°, 150°)$ or $\lvert\gamma-\beta\rvert \in [210°, 240°)$	15.089
~~H~~Anticlinal slope	$\alpha > 5°$, $\lvert\gamma-\beta\rvert \in [150°, 210°)$	14.857

Stratigraphic lithology data was obtained by vectorizing and classifying geological maps ~~(scale~~at a 1:200,000~~).~~ scale. Each lithology ~~has a different~~is associated with distinct pedogenic ~~environment and will vary~~environments, leading to variations in composition and stability, which ~~affects the~~ in turn influence landslide occurrence ~~of landslides~~ (Cobos-Mora et al., 2023). In this ~~paper, the~~ study, the area ~~is~~was classified into four lithological categories: carbonate, clastic, carbonate and clastic, as well as ~~Igneous~~igneous and metamorphic rocks. ~~In addition, when the research area is~~ Furthermore, in large ~~and most of the tectonics are~~ study areas where tectonic features are highly intertwined ~~with each other~~, the distance ~~from tectonics is no longer suitable~~to tectonic structures becomes less relevant as a ~~correlation~~correlating factor~~, and~~; instead, tectonic density should be ~~used instead~~considered (Wang et al., 2014). ~~Also, since the road data also show interlocking status, this paper uses tectonic density and road density as evaluation factors. When using ArcGIS to calculate the density, the search radius is kept as default, and the area unit is square kilometers.~~

To ensure the ~~reasonableness of the~~ rational selection of landslide~~-~~-inducing factors, ~~this study used~~ Pearson correlation analysis was employed to ~~explore~~examine the degree of correlation among the selected ~~inducing~~ factors (Zhang et al., 2022) (Fig. ~~1~~39). The ~~value of~~ correlation coefficient ranges from -1 to 1~~. The~~, where values closer ~~the value is~~ to 1 or -1~~, the~~ indicate a stronger ~~the~~ correlation between the ~~two~~ variables, and ~~the~~values closer ~~the value is~~ to 0~~, the~~ indicate a weaker ~~the~~ correlation ~~between the two variables~~ (Cao et al., 2023).

~~The~~As shown in Fig. 9, the correlation coefficients between ~~the~~most inducing factors are low, ~~as shown in Fig. 13,~~ with the exception of ~~the~~a somewhat higher correlation ~~value~~ between elevation and river distance (0.53). ~~Given that elevation~~ Elevation and river distance are ~~two important~~both critical factors ~~for causing landslides (~~in landslide occurrence—elevation is ~~inherent in the~~fundamental to landslide susceptibility assessment ~~of LS~~ (Wang et al., 2022b), ~~which affects~~affecting the distribution of submerged layers ~~as well as~~and the intensity of human activities; ~~and the erosive effect of the~~while river ~~on the shoreline~~erosion can ~~damage~~destabilize slopes by undercutting the ~~foot of the slope~~base and ~~soften the~~softening rock and soil ~~mass~~masses (Selamat et al., 2022)~~), they are all~~). Therefore, both factors were retained in this study. ~~These~~Ultimately, 11 inducing factors were ~~finally determined to be used in the TGRA's LS~~selected for landslide susceptibility assessment ~~research~~in the study area.

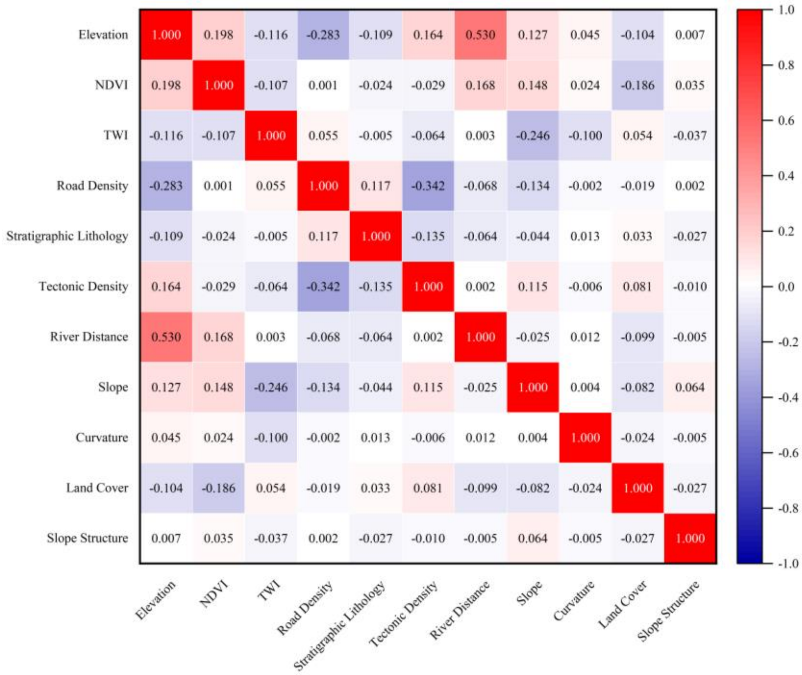

Figure 9: Pearson correlation analysis results for landslide-inducing factors.

4.2.2 Grading of Landslide Susceptibility Factors

~~Combined with~~Considering the ~~actual situation~~specific conditions of the study area and ~~the results of~~insights from previous ~~studies~~research, the ~~class~~ classification of each landslide predisposing factor ~~and~~, along with the corresponding result map ~~of this study are shown~~, is presented in Table 7 and Fig. ~~14~~10. The landslide susceptibility evaluation was ~~carried out in~~conducted using raster cells with ~~a size~~dimensions of 30m × 30m. ~~It's also worth noting~~It is important to emphasize that the historical landslide data ~~utilized~~used for ~~LS~~susceptibility prediction ~~includes~~encompasses all 6,888 recorded ~~landslides~~landslide events, not just the 453 events filtered for inclusion in the ~~RTM~~rainfall threshold model calculations.

Table 7: Classification of landslide-inducing factors used in this study.

Predisposing Factor	Classification Criteria	Code
Elevation (m)	≤300	a
	(300,600]	
	(600,900]	
	(900,1200]	
	(1200,1500]	
	>1500	
NDVI	[-1,0]	b
	(0,0.2]	
	(0.2,0.4]	
	(0.4,0.6]	
	(0.6,0.8]	
	(0.8,1]	
TWI	≤6	c
	(6,8]	
	(8,10]	
	(10,14]	
	>14	
Road Density (km/km^2)	[0,0.5]	d
	(0.5,1.2]	
	(1.2,2.5]	
	(2.5,5.0]	
	>5.0	
Stratigraphic Lithology	Carbonates	e
	Clastic rocks	
	Carbonates and clastic rocks	
	Igneous and metamorphic rocks	
Tectonic Density (km/km^2)	[0,0.03]	f
	(0.03,0.12]	
	(0.12,0.24]	
	(0.24,0.38]	
	>0.38	
River Distance (m)	≤500	g
	(500,1000]	
	(1000,1500]	
	>1500	
Slope (°)	[0,10]	h
	(10,20]	
	(20,30]	

	(30,40] (40,50] >50	
Curvature (m^{-1})	≤-3 (-3,-1] (-1,0] (0,1] >1	i
Land Cover	Urban land Agricultural land Forest land Grassland Water Other Land	j
Slope Structure	~~A~~Nearly horizontal slope ~~B~~Over-dip slope ~~D~~Under-dip slope ~~E~~Dip-oblique slope ~~F~~Transverse slope ~~G~~Anticlinal-oblique slope ~~H~~Anticlinal slope	k

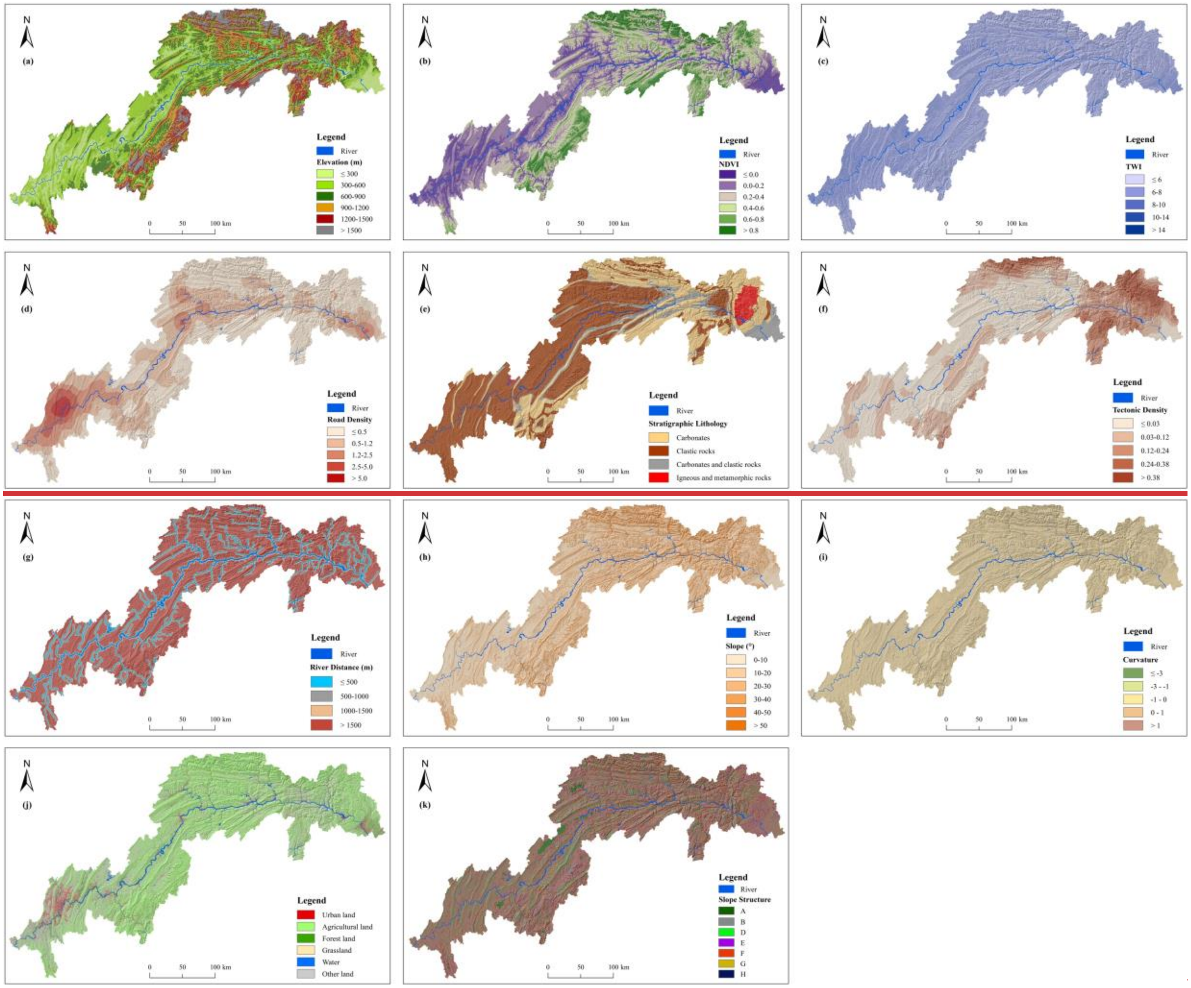
(a)
Legend
River
Elevation (m)
≤ 300
300-600
600-900
900-1200
1200-1500
> 1500
0 50 100 km
(b)
Legend
River
NDVI
≤ 0.0
0.0-0.2
0.2-0.4
0.4-0.6
0.6-0.8
> 0.8
(c)
Legend
River
TWI
≤ 6
6-8
8-10
10-14
> 14
(d)
Legend
River
Road Density
≤ 0.5
0.5-1.2
1.2-2.5
2.5-5.0
> 5.0
(e)
Legend
River
Stratigraphic Lithology
Carbonates
Clastic rocks
Carbonates and clastic rocks
Igneous and metamorphic rocks
(f)
Legend
River
Tectonic Density
≤ 0.03
0.03-0.12
0.12-0.24
0.24-0.38
> 0.38
(g)
Legend
River
River Distance (m)
≤ 500
500-1000
1000-1500
> 1500
(h)
Legend
River
Slope (°)
0-10
10-20
20-30
30-40
40-50
> 50
(i)
Legend
River
Curvature
≤ -3
-3 - -1
-1 - 0
0 - 1
> 1
(j)
Legend
Urban land
Agricultural land
Forest land
Grassland
Water
Other land
(k)
Legend
River
Slope Structure
A
B
D
E
F
G
H

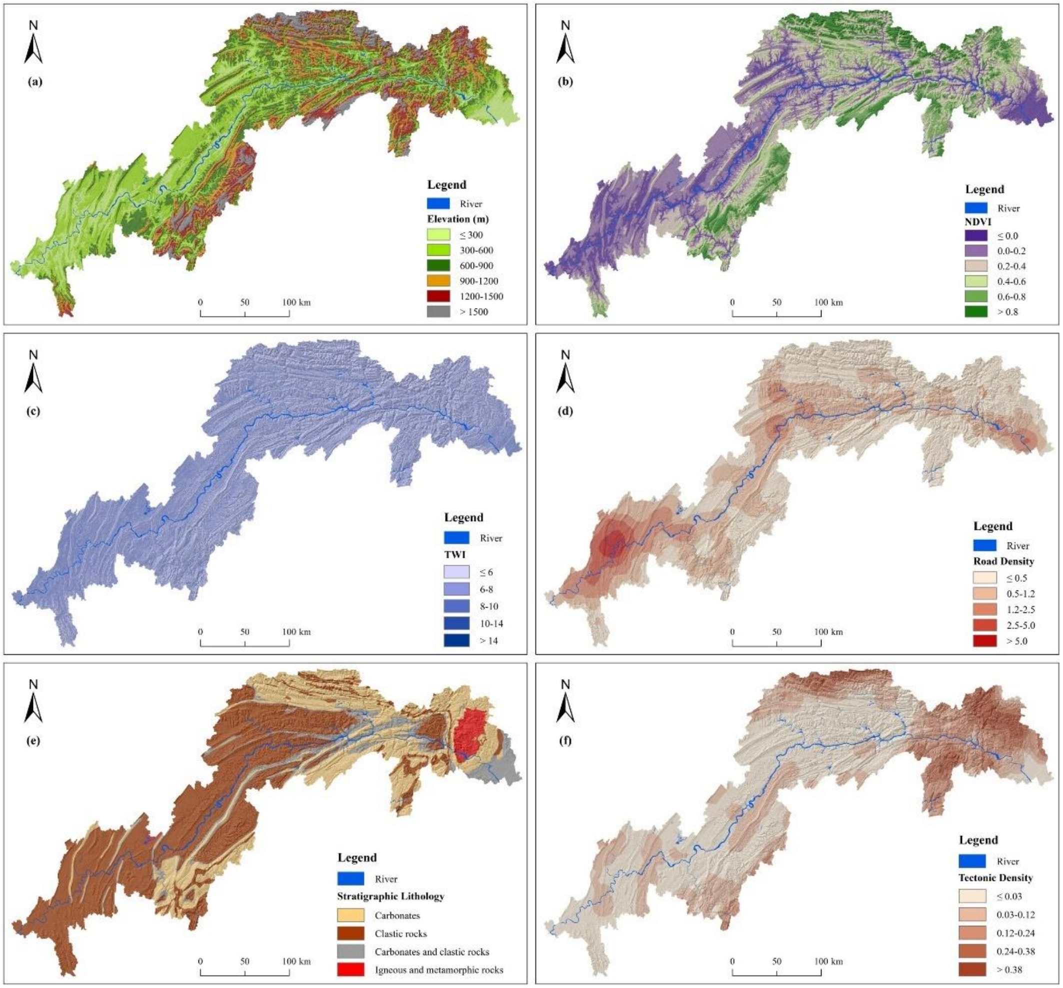

Figure ~~14: Landslide~~ 10-1: Grading results for landslide-inducing factors~~ grading results map~~. (a) Elevation; (b) NDVI; (c) TWI; (d) Road density; (e) Stratigraphic lithology; (f) Tectonic density.

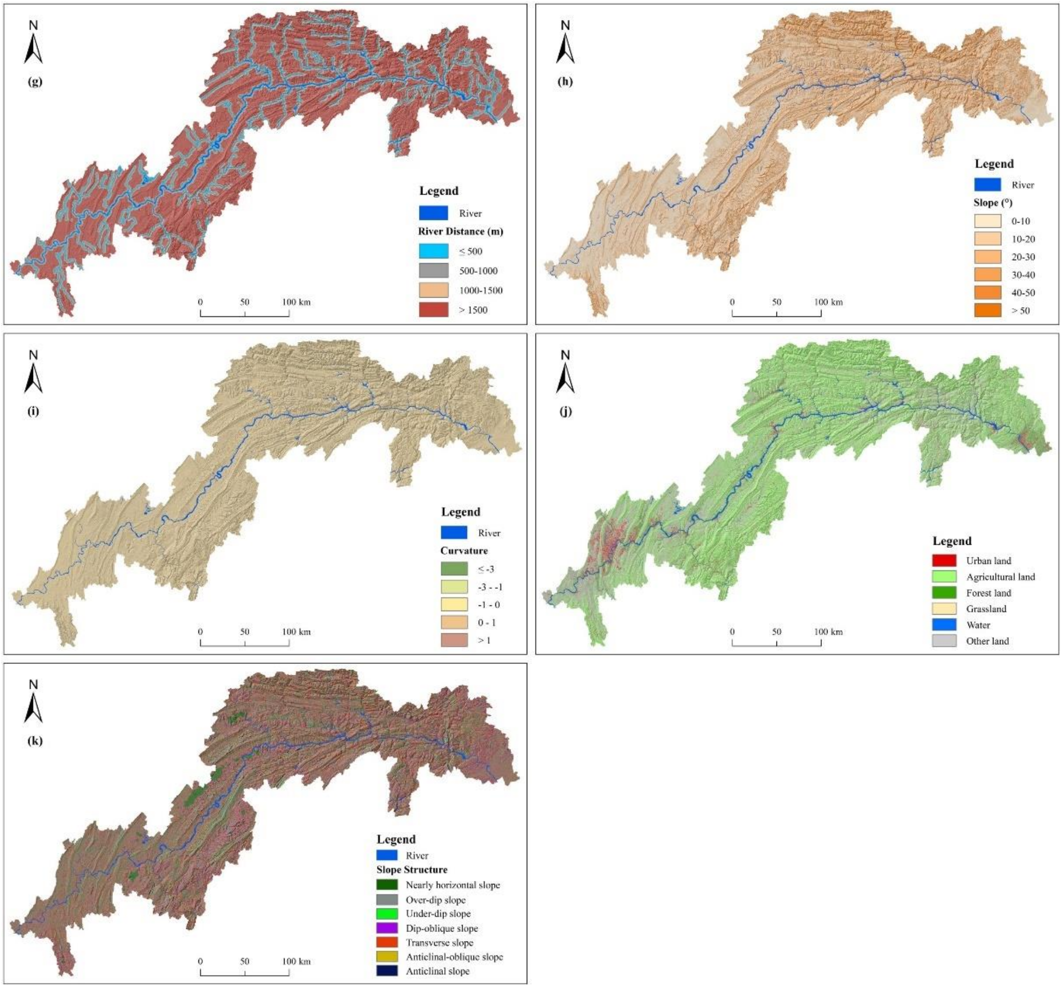

Figure 10-2: Grading results for landslide-inducing factors (continued). (g) River distance; (h) Slope; (i) Curvature; (j) Land cover; (k) Slope structure.

4.2.3 Landslide Susceptibility Evaluation Results

In this study, three models, CNN-3D, RF and SVM, were ~~used~~employed to evaluate the ~~LS~~landslide susceptibility of the study area~~, and the~~. The optimal ~~LS result was chosen~~landslide susceptibility results obtained from these models were then selected for subsequent daily ~~LHW.~~landslide hazard warnings. The relevant ~~indicators obtained~~performance metrics from the training of the three models are ~~shown~~presented in Table 8.

Table 8 indicates that the AUC values for the CNN-3D, RF, and SVM models are 0.96, 0.82, and 0.83, respectively. These AUC values demonstrate that all three models effectively predict the probability of landslide occurrence in the study area, with the CNN-3D model exhibiting superior predictive accuracy compared to the RF and SVM models. Furthermore, the CNN-3D model outperforms the RF and SVM models across the other four metrics. Consequently, the landslide susceptibility results from the CNN-3D model were classified into five categories using the natural breaks method (Fig. 11) and were subsequently utilized for daily landslide hazard warnings.

Table 8: Results ~~of~~from the training of the susceptibility evaluation ~~model~~models.

Model	Model Evaluation Indicators				
	AUC	Accuracy	Precision	Recall	F1_score
CNN-3D	0.96	0.9003	0.8663	0.9295	0.8968
RF	0.82	0.7500	0.7656	0.7416	0.7534
SVM	0.83	0.7630	0.7625	0.7623	0.7624

~~Table 8 shows that the AUC values for CNN-3D, RF, and SVM models are 0.96, 0.82, and 0.83, respectively. The AUC values indicate that all three models can better predict the probability of landslide occurrence in the study area, but the CNN-3D model has a greater prediction accuracy than the RF and SVM models. In addition, for the other four metrics, the CNN-3D model outperforms the RF and SVM models. As a consequence, in this study, the CNN-3D model's LS result was divided into five classes using the natural breaks approach (Fig. 15) and was used for subsequent daily LHW.~~

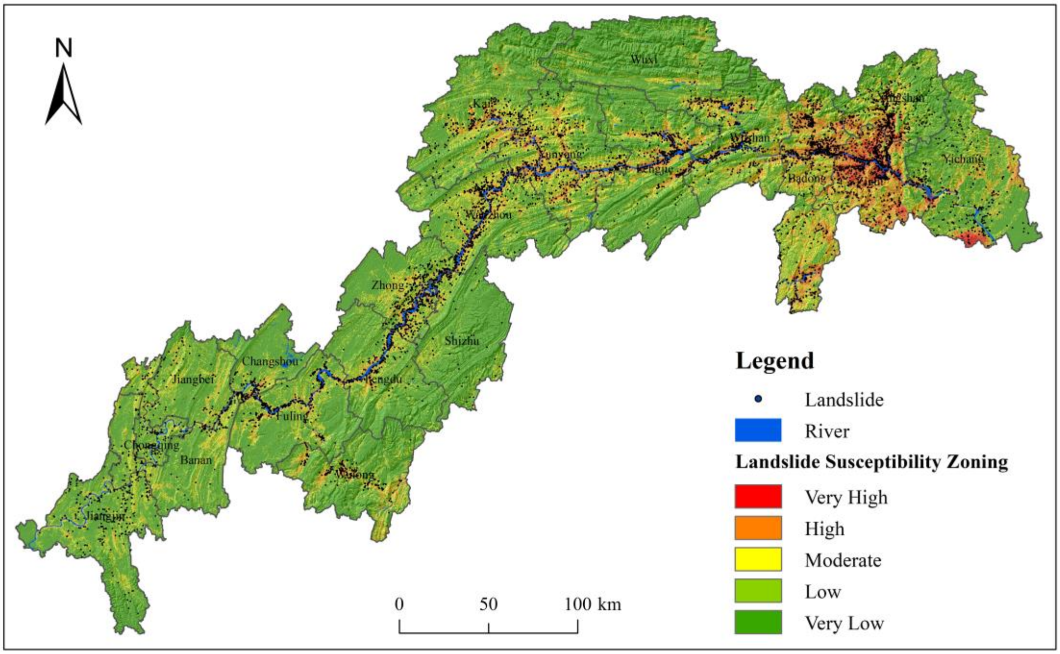

Figure ~~15: CNN-3D model landslide~~11: Landslide susceptibility results from the CNN-3D model.

~~As a whole, the~~ Overall, areas of high landslide ~~disaster high~~ susceptibility ~~areas~~ in the study ~~area~~region are ~~mainly concentrated~~predominantly located along ~~the~~ riverbanks and in the central and eastern ~~regions. In terms of~~ sections. Within the district and county ~~scopes, the landslide disaster~~boundaries, high susceptibility areas are ~~mainly~~primarily concentrated

~~at~~in Zigui, the northern part of Badong, the southern part of Xingshan, the central part of Fengjie, the central part of Wanzhou, and the southeastern part of Zhongxian.

4.3 Landslide Hazard Warning

4.3.1 Landslide Hazard Results for Each Rainfall Warning Level

In this study, a superposition matrix (Table 9) was created to ~~couple the daily RWL with the LS result to generate the daily LHW result. Based on the superimposed matrix, four categories of landslide hazard levels will be obtained, where 1 indicates relatively stable zone, 2 indicates general prevention zone, 3 indicates secondary prevention zone, and 4 indicates priority prevention zone~~integrate the daily rainfall warning level with the landslide susceptibility results, thereby generating daily landslide hazard warnings.

Table 9: ~~Landslide~~Superposition matrix of landslide susceptibility and rainfall warning ~~level superposition matrix~~levels. In the table, the numerical codes represent the following zones: 1 – Relatively stable zone, 2 – General prevention zone, 3 – Secondary prevention zone, and 4 – Priority prevention zone.

Susceptibility / Rainfall Threshold Level	Very Low	Low	Moderate	High	Very High
Caution	1	1	1	1	2
Special Caution	1	1	1	2	3
Warning	1	1	2	3	4
Severe Warning	1	2	3	4	4

Based on the ~~LS~~landslide susceptibility results ~~shown~~depicted in Fig. ~~15, combined with~~ 11 and utilizing the superposition matrix from Table 9, the ~~LHW results~~landslide hazard warning outcomes corresponding to each rainfall level were ~~obtained~~determined (Fig. ~~16~~12).

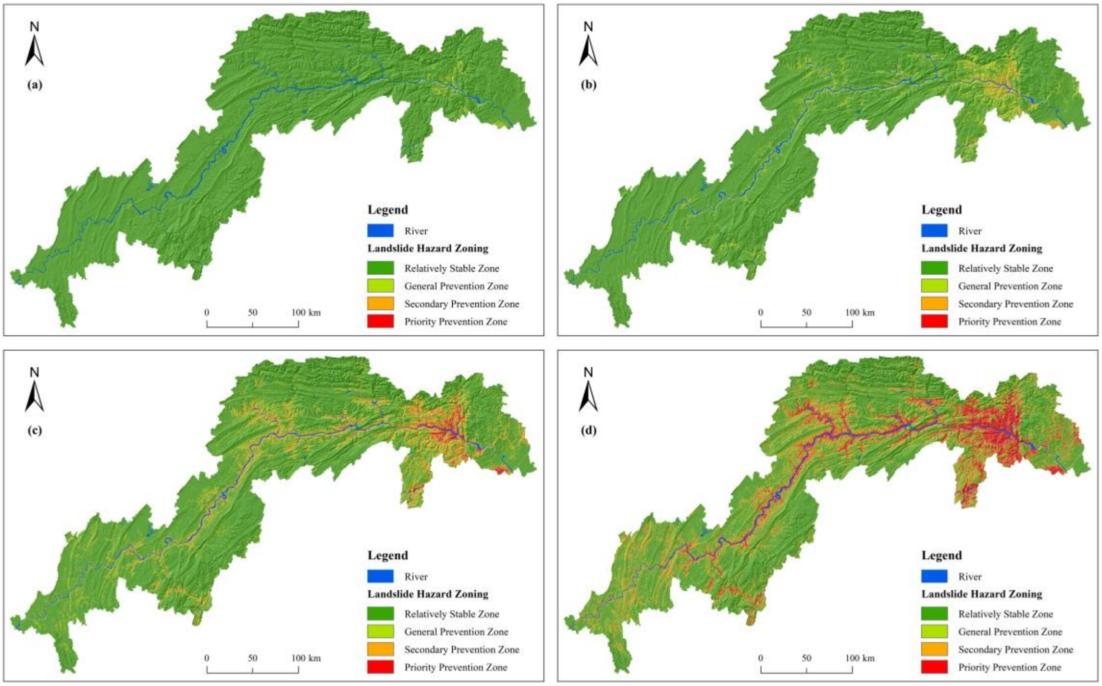

Figure ~~16~~12: Landslide hazard maps for each rainfall warning level. (a~~. attention~~) Attention level hazard; (b~~. special~~) Special attention level hazard; (c~~. warning~~) Warning level hazard; (d~~. severe~~) Severe warning level hazard~~)~~.

4.3.2 Daily Landslide Hazard Warning

In 2020, the Yangtze River experienced its worst basin-wide flood since 1998. ~~on~~On July 19, the "Yangtze River Flood No. 2 of 2020" was ~~progressing~~advancing through the ~~TGRA to~~ study area toward the middle and lower reaches of the ~~Yangtze River, and the~~ river, leading to persistent rainfall ~~induced many~~and numerous landslides. ~~Therefore, in this study~~Thus, 19 July, 2020 was ~~used~~selected as ~~an example~~a case study for ~~LHW~~ landslide hazard warning and validation~~. Based on the anticipated rainfall data at~~ (Fig. 13). Using the superposition matrix in Table 9, Fig. 13.d was overlaid on Fig. 12 to derive the ~~time, E and D~~landslide hazard warning results for ~~the rainfall forecast stations from 14~~19 July, 2020 ~~to 18 July 2020, and R for 19 July 2020, were calculated. Kriging interpolation was used to generate E (Fig. 17.a) and R (Fig. 17.b) for the whole research region. Since D is an integer ranging from 0 to 5, interpolation cannot be used to acquire D for the whole research region; thus, this study uses the Thiessen polygon method and feature to raster method to obtain D for the entire study area (Fig. 17.c).The RWL for 19 July 2020 was calculated per sub-region~~ (Fig. ~~17.d) using the optimum RTM for each sub-region obtained above (Table 4~~14).

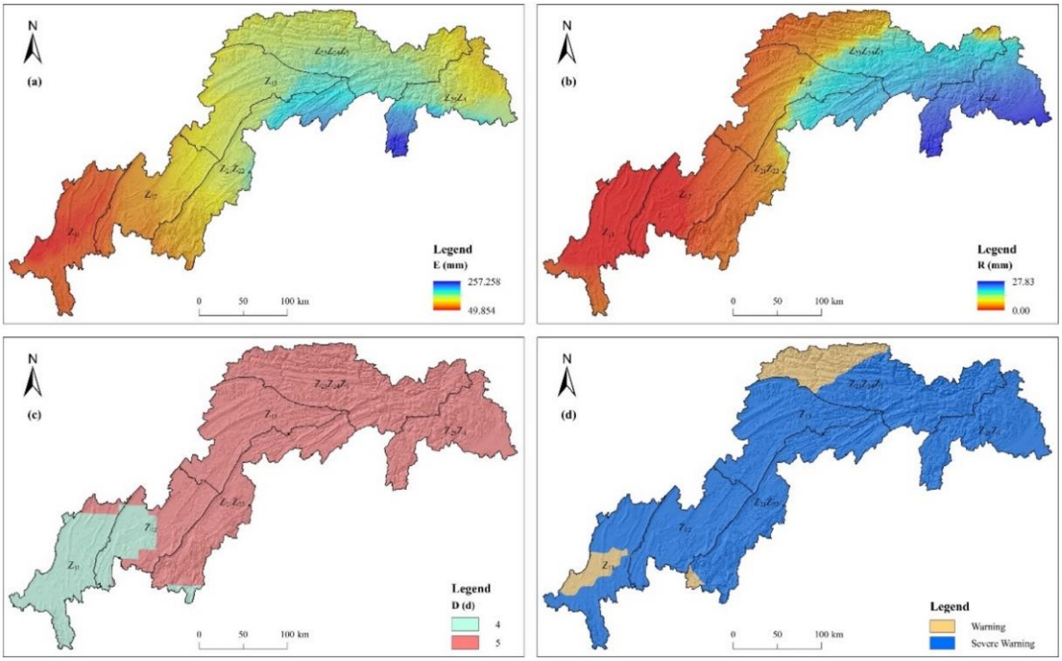

Figure ~~17~~13: Various rainfall parameters and rainfall warning levels for ~~19 July 2020~~July 19, 2020. (a) Effective rainfall interpolated by Kriging; (b) Daily rainfall interpolated by Kriging; (c) Duration of rainfall estimated using Thiessen polygons; (d) Rainfall warning levels calculated using the optimal rainfall threshold model.

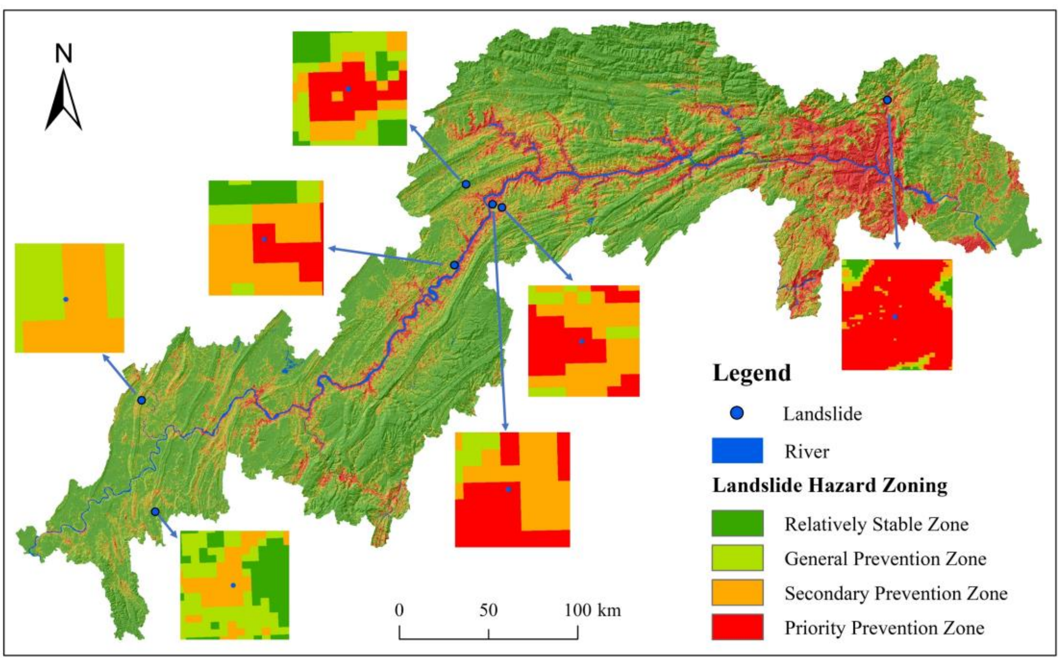

Figure ~~Figure 18~~14: Landslide hazard warning results for 19 July, 2020.

On July 19, 2020, ~~there were~~ seven landslide hazards were identified, as ~~shown~~depicted in Fig. ~~18. Five of them fell in~~14. Of these, five were classified within the priority prevention zone, and two ~~in~~within the secondary prevention zone, ~~demonstrating~~which confirms the accuracy of both the ~~LHW~~landslide hazard warning results and the rainfall threshold model.

5. Discussion

5.1 Discussion of Rainfall Threshold Model

To ~~investigate~~identify the ~~best~~most effective rainfall thresholds in the ~~TGRA,~~study area, this study employs two regression methods, OLS and MLP, ~~and~~alongside two ~~RTM~~rainfall threshold models, E-D and E-D-R~~, are used in this study.~~. Regardless of the regression ~~approach~~method used, the results reveal that the E-D-R model ~~has greater~~exhibits superior warning accuracy ~~than~~compared to the E-D model. ~~In addition~~Additionally, the optimal ~~RTM~~rainfall threshold models for ~~two areas,~~the Z_{13} and $Z_{23}Z_{24}Z_{3}$~~,~~ areas are the E-D-R models ~~obtained~~derived from the MLP regression, ~~indicating~~demonstrating the ~~feasibility~~viability of ~~using~~ neural networks (MLP) ~~for the study of RTM.~~ in rainfall threshold modeling. However, ~~since~~given that the dataset ~~of~~in this study is ~~not large (~~relatively small (comprising only 453 landslides) ~~nor complex (~~and simple (involving only 3 variables), it may not ~~be able to clearly demonstrate~~fully capture the advantages of neural networks for rainfall threshold modeling. ~~But~~Nevertheless, we ~~believe that~~consider this ~~is~~ a valuable ~~attempt, and more~~effort. Future studies could incorporate additional variables, such as peak rainfall and rainfall intensity ~~can be added in subsequent studies, and the application of~~, and applying neural networks ~~will certainly improve~~is likely to enhance the accuracy of ~~RWM~~rainfall warning models.

To explore the reasons for the E-D-R model's ~~higher~~superior warning accuracy, this study ~~uses~~examines area Z_{12} as ~~an example,~~a case study and ~~shows some of the~~illustrates points where the ~~RWL~~ rainfall warning level has been ~~changed~~modified (i.e. landslides ~~where the RWL has been~~with increased warning levels) in the R-E plane view (Fig. ~~19), where the colors of the landslides indicate the different RWL,~~15).

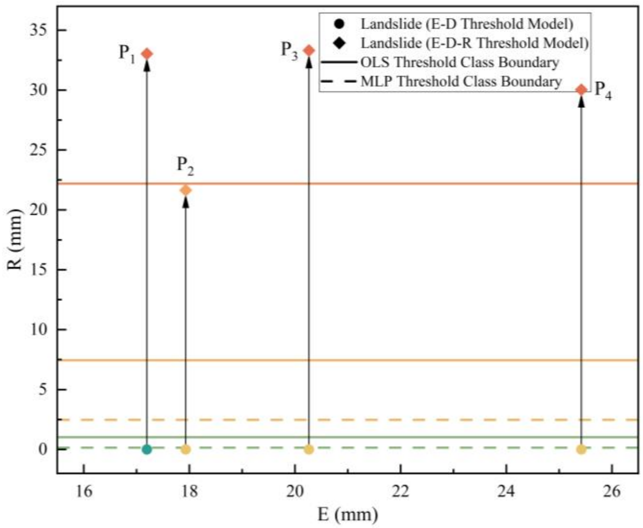

Figure 15: Transition process of rainfall warning levels in the Z_{12} region. The green line indicates the boundary between the Special Attention and Attention levels, the yellow line denotes the boundary between the Warning and ~~the meaning is the same as in Fig. 12~~Special Attention levels, and the orange line marks the boundary between the Severe Warning and Warning levels.

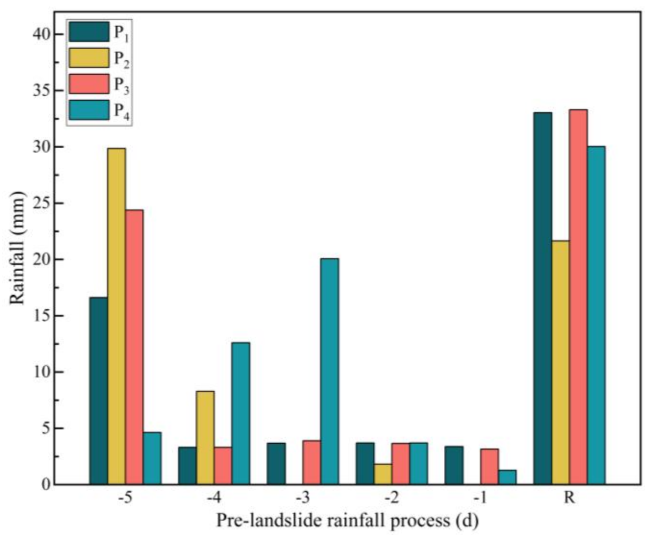

Figure ~~19~~16: Rainfall ~~warning level~~processes at the transition ~~process (Z_{12} region).~~points of rainfall warning levels.

The chart ~~shows~~illustrates that ~~after~~ the inclusion of the R indication ~~was added, the RWL of the four landslides rose dramatically. The~~significantly elevated the rainfall warning level ~~of P_1 in~~ for the four landslides. In the E-D model, P_1 was ~~only~~classified as “Caution”, ~~and~~while the ~~warning levels of the remaining~~other three landslides were ~~only~~categorized as “Special Caution”~~, whereas~~. However, in the E-D-R model ~~using~~with OLS regression, the warning level of P_2 was ~~raised~~upgraded to “Warning”, and the warning levels of the remaining three landslides were ~~raised~~elevated to “Severe Warning”. Similarly, ~~the alert levels of~~ all four ~~landslip points~~landslides were ~~raised~~classified to “Warning” in the E-D-R model using the MLP regression~~ method. These~~. The transitions in rainfall warning levels for these landslides ~~with RWL~~

~~transition were~~directly contributed to the ~~direct reason of the E-D-R model's~~ improved accuracy of the E-D-R model in the Z_{12} region.

~~Further exploration~~An in-depth analysis of the rainfall ~~process of~~processes for these four landslides ~~before the landslide occurred~~prior to their occurrence (Fig. ~~20~~16) reveals that ~~these four landslides received less~~they experienced relatively low rainfall in the four days ~~before~~leading up to the landslide, resulting in a lower E value, but ~~more~~substantial rainfall on the day of the landslide. ~~The above~~These characteristics ~~make these four landslides have~~ resulted in higher warning accuracy ~~in~~for these four landslides within the E-D-R ~~RTM, indicating~~rainfall threshold model, suggesting that the R indicator ~~R~~ has ~~some~~notable sensitivity ~~in terms of~~to landslides ~~caused~~triggered by heavy ~~rain.~~rainfall.

5.2 Discussion of Daily Landslide Hazard Warning

In this study, RF, SVM, and CNN-3D models were used to predict ~~LS~~landslide susceptibility in the ~~TGRA, and a comparison of the three models' results showed~~Three Gorges Reservoir Area. A comparative analysis revealed that the CNN-3D model ~~predicts LS with more~~offers superior predictive accuracy ~~in~~for landslide susceptibility within the study area. ~~In addition, further analysis~~ Further examination of the CNN-3D model's ~~LS~~ results show that the ~~very~~regions with high ~~LS zone is primarily distributed~~landslide susceptibility are predominantly located in areas with sparse vegetation, fragile stratigraphic lithology, close to rivers, and active human engineering activities, which is similar with the results ~~of~~reported by Wang et al (~~Wang et al.,~~ 2022a).

~~In terms of~~Regarding daily ~~LHW, RWL are~~ landslide hazard warnings, rainfall warning levels were calculated using the optimal ~~RTM~~rainfall threshold model for each sub-district based on forecast rainfall data from rainfall stations. ~~Subsequently, the~~ The daily ~~LHW~~landslide hazard warning results were ~~derived~~ then generated by ~~utilizing~~employing a superposition matrix to ~~combine~~integrate the rainfall warning levels with the ~~RWL and LS~~landslide susceptibility results. On July 19, 2020, all seven identified landslide hazards ~~are~~were confirmed to be ~~in~~within the priority ~~prevention~~ and secondary prevention zones. ~~It can be observed~~This indicates that the ~~LHW~~landslide hazard warning results ~~obtained through the RTM have very high accuracy and are of great significance in the~~derived from the rainfall threshold model are highly accurate and significantly contribute to effective landslide disaster prevention and control~~ of landslide disasters. In addition~~. Moreover, the process of ~~transforming the LS~~translating landslide susceptibility results into ~~LHW results~~hazard warnings through the ~~RWL~~rainfall warning levels and superposition matrix ~~is essentially~~serves as a refinement mechanism. This correction ~~process of the LS results. After the correction,~~reduces the areas ~~that need to be~~requiring focused ~~on~~ prevention and attention ~~can be reduced to a certain extent, which saves the cost of manpower and material~~ , thereby optimizing the allocation of resources ~~in~~for landslide ~~prevention~~management.

It is also important to note that the spatial probability of landslide occurrence may vary between dry and rainy seasons, and the influence of different landslide-inducing factors may change under varying climatic conditions. This study primarily focused on the differences in rainfall thresholds across various climatic and ~~control~~topographic conditions, while the variations in spatial probability of landslide occurrence were not extensively explored. Additionally, changes in reservoir water levels and groundwater fluctuations in the Three Gorges Reservoir Area are significant factors influencing landslide occurrence; however, these factors were not included in this study due to data limitations.

5.3 Practical Application of the Rainfall Threshold Model and Daily Landslide Hazard Warning

In the ~~actual~~practical prevention and control of landslide hazards, ~~it is~~ cost considerations are inevitable ~~to consider the factor of cost~~ (Wang et al., 2023a). To ~~safeguard as many people's~~maximize the protection of lives and property ~~as possible~~ within ~~the limited cost range~~a constrained budget, it is ~~necessary~~essential to ~~narrow~~prioritize and refine the ~~regions~~areas that ~~must be prioritized~~require focused attention, while ~~guaranteeing~~maintaining the accuracy of ~~the LHW~~ landslide hazard warning results.

The E-D-R ~~RTM, while considering the advantages~~rainfall threshold model, by incorporating the benefits of the E-D ~~RTM, increases the~~model, enhances sensitivity to landslides induced by heavy rainfall on the same day~~,~~ and ~~has~~achieves higher ~~landslide~~ warning accuracy. ~~Meanwhile~~Concurrently, the CNN-3D model ~~fully considers the~~, which effectively integrates spatial information around each raster point, ~~and its predicted LS results have higher prediction accuracy than those of~~ provides more accurate landslide susceptibility predictions compared to the RF and SVM models. ~~Therefore,~~Thus, both the E-D-R ~~RTM~~rainfall threshold model and the CNN-3D model ~~have a broad~~ hold significant potential for application ~~space~~ and development ~~prospect~~ in ~~the~~landslide warning and prevention ~~of landslide disasters.~~. The ~~LHW~~combination of these models' results ~~obtained by~~through superposition ~~of the results of the two models~~ can ensure high accuracy ~~and at the same time narrow down the areas that need to be focused on by virtue of the RWL results obtained by the RTM, so as to~~in landslide hazard warnings while also narrowing the focus areas using the rainfall warning levels derived from the rainfall threshold model. This approach helps meet the ~~requirements~~demands of effective landslide disaster prevention and control ~~work~~.

~~In addition, although the~~ Nevertheless, despite the high accuracy of the E-D-R ~~RTM as well as~~ rainfall threshold model and the CNN-3D model ~~have high accuracy, there are~~, certain uncertainties persist. For the ~~RTM~~rainfall threshold model: (1) ~~The rainfall station can only accurately reflect the rainfall situation of the site~~Rainfall stations provide localized data, and there ~~will~~may be inaccuracies ~~and uncertainties whether the rainfall~~when extending this data ~~are extended~~ to the ~~whole~~entire study area ~~by~~using interpolation or Thiessen polygon ~~method~~methods. (2) Historical landslide data ~~play a decisive~~significantly influence ~~on~~ the results of the rainfall threshold model~~. Either less historical landslide~~; insufficient data or ~~the existence of more~~ extreme rainfall conditions ~~will~~can lead to ~~uncertainty~~uncertainties in the final ~~RWL.~~rainfall warning levels. (3) Although this study ~~divided~~analyzed 10 regions ~~as well as~~across both dry and rainy seasons ~~for the rainfall threshold study, the overall~~, the broad regional scope ~~is still large. There will be some~~introduces uncertainty in ~~the~~ rainfall thresholds ~~for different topography~~due to varying topographic and ~~geomorphology in the region~~geomorphological conditions. For the CNN-3D model, uncertainties may arise from the selection of landslide-inducing factors, the size of the evaluation unit, and the division ratio of the training ~~set~~and test set~~, and so on, will produce uncertainty~~.

Therefore, in practical~~ application of~~ landslide prevention and control applications, it is ~~necessary~~crucial to ~~combine~~tailor the ~~actual situation of the local area and select appropriate~~ predisposing factors ~~as well as~~and evaluation units to the specific local context to ensure the accuracy of the ~~LS~~landslide susceptibility results (Zhang et al., 2023). Simultaneously, ~~a~~constructing a comprehensive historical landslide database ~~can~~is recommended. This database should be ~~constructed. When a~~updated with new landslide ~~occurs, the~~events and corresponding rainfall data ~~will be summarized into~~to recalibrate the ~~database and the~~area's rainfall threshold ~~of~~and refine the rainfall warning levels. As the historical landslide data accumulate, the ~~area will be recalculated for the subsequent RWL. The~~ uncertainty ~~of~~in the ~~RTM~~rainfall threshold model is expected to ~~reduce as the quantity of historical landslide data grows, and the~~decrease, leading to more precise rainfall thresholds~~ will continue to converge to the ultimate rainfall thresholds for the region. Furthermore, when the historical landslide data are~~ . With a sufficiently rich~~, the region may be split~~ historical dataset, further ~~to constantly~~ regional subdivision may enhance rainfall warning accuracy. Ultimately, this approach will improve the ~~accuracy of the rainfall warning level. Ultimately, the accuracy of LHW will be increased to give~~precision of landslide hazard warnings and provide valuable technical ~~assistance for subsequent assessment of~~ support for vulnerability ~~as well as~~assessment and disaster preventive and mitigation efforts.

6. Conclusion

Landslide disaster warning is ~~an essential~~a critical tool ~~in~~for the prevention and management of landslides. To ~~improve~~enhance the accuracy of landslide warning, this ~~paper first chose~~study employed two regression methods~~, ~~—MLP and OLS~~, ~~—and two ~~RTM, ~~rainfall threshold models—E-D and E-D-R~~, and~~. The study area was divided ~~the TGRA~~ into two seasons, dry and rainy~~ seasons~~, as well as several sub-districts based on topography and rainfall patterns, to ~~explore~~identify the optimal ~~RTM~~rainfall threshold model for the ~~study area~~region and ~~obtain~~determine the daily ~~RWL. Subsequently~~rainfall warning levels. Additionally, 11 inducing factors were selected to ~~investigate the LS in~~ assess landslide susceptibility in the study area ~~utilizing~~using three models: RF, SVM, and CNN-3D. ~~Finally,~~ The final step involved integrating the rainfall warning levels with the landslide susceptibility results using a superposition matrix~~, the RWL was overlaid on the LS results~~ to ~~achieve~~produce daily ~~LHW in the TGRA~~landslide hazard warnings for the Three Gorges Reservoir Area.

~~In terms of rainfall threshold models, the study's~~The results ~~suggest~~indicate that the E-D-R ~~RTM has~~rainfall threshold model exhibits superior sensitivity ~~in terms of~~to landslides ~~induced~~triggered by heavy rainfall, ~~therefore the~~ resulting in higher rainfall warning accuracy ~~produced by~~compared to the E-D model when either regression method is ~~higher than that of the E-D model. In addition, for each~~ applied. Specifically, for sub-district~~, the optimal RTM for the four zones~~ Z_{11}, Z_{12}, $Z_{21}Z_{22}$, $Z_{25}Z_{4}$, and Dry Season, the optimal rainfall threshold model is the E-D-R ~~RTM calculated by~~ model derived from OLS regression~~; whereas the optimal RTM for the two zones~~. Conversely, for sub-districts Z_{13} and $Z_{23}Z_{24}Z_{3}$, the optimal model is the E-D-R ~~RTM~~threshold obtained ~~by~~through MLP regression. ~~In terms of LS~~Regarding landslide susceptibility, the CNN-3D ~~model's AUC and Accuracy~~model achieved an AUC of 0.96 and an accuracy of 0.9003, ~~respectively, and its prediction accuracy~~ outperformed the RF and SVM models in prediction accuracy.

~~The daily LHW is~~ Daily landslide hazard warnings were calculated by combining the daily ~~RWL and~~ rainfall warning levels with the landslide susceptibility results. ~~Data from the 19~~ The accuracy of these warnings was validated using data from the landslide event on July 19, 2020 ~~hazard event were utilized to verify the LHW results in this research~~. Of the seven ~~landslide hazards~~landslides on that date, five ~~fell~~occurred in the priority prevention zone and two in the secondary prevention zone, ~~proving the accuracy~~confirming the reliability of the landslide hazard warning results and the effectiveness of the ~~LHW~~rainfall threshold model.

The integration of rainfall warning levels with landslide susceptibility results provides actionable guidance ~~and reference~~ for local landslide disaster prevention and control ~~operations. In addition~~efforts. Moreover, the introduction of MLP ~~to~~into the regression analysis of rainfall ~~threshold~~thresholds in this study ~~also further enriches~~contributes to the ~~calculation method~~development of ~~RTM, which is of some significance~~rainfall threshold models and offers a valuable approach for ~~promotion~~broader application.

Code and data availability

The data and code can be accessed at https://doi.org/10.5281/zenodo.11311851 (Peng, 2024).

Author contributions

Bo Peng: Writing - original draft, Writing - review & editing, Data curation, Formal analysis, Validation.

Xueling Wu: Writing - review & editing, Funding acquisition, Conceptualization, Methodology.

Competing interests

The authors declare that they have no conflict of interest.

Disclaimer

Publisher's note: Copernicus Publications remains neutral with regard to jurisdictional claims made in the text, published maps, institutional affiliations, or any other geographical representation in this paper. While Copernicus Publications makes every effort to include appropriate place names, the final responsibility lies with the authors.

Acknowledgements

This study was supported by the National Natural Science Foundation of China (42071429).

Reference

Abraham, M.T., Pothuraju, D., Satyam, N., 2019. Rainfall Thresholds for Prediction of Landslides in Idukki, India: An Empirical Approach. Water 11, 16.

Abraham, M.T., Satyam, N., Kushal, S., Rosi, A., Pradhan, B., Segoni, S., 2020a. Rainfall Threshold Estimation and Landslide Forecasting for Kalimpong, India Using SIGMA Model. Water 12, 13.

Abraham, M.T., Satyam, N., Pradhan, B., Alamri, A.M., 2020b. Forecasting of Landslides Using Rainfall Severity and Soil Wetness: A Probabilistic Approach for Darjeeling Himalayas. Water 12, 19.

Aksha, S.K., Resler, L.M., Juran, L., Carstensen, L.W., 2020. A geospatial analysis of multi-hazard risk in Dharan, Nepal. Geomat. Nat. Hazards Risk 11, 88-111.

Baharvand, S., Rahnamarad, J., Soori, S., Saadatkhah, N., 2020. Landslide susceptibility zoning in a catchment of Zagros Mountains using fuzzy logic and GIS. Environ. Earth Sci. 79, 10.

Barcenas, O.U.E., Pioquinto, J.G.Q., Kurkina, E., Lukyanov, O., 2023. Surrogate Aerodynamic Wing Modeling Based on a Multilayer Perceptron. Aerospace 10, 19.

Budimir, M.E.A., Atkinson, P.M., Lewis, H.G., 2015. A systematic review of landslide probability mapping using logistic regression. Landslides 12, 419-436.

Cao, J.S., Qin, S.W., Yao, J.Y., Zhang, C.B., Liu, G.D., Zhao, Y.Y., Zhang, R.C., 2023. Debris flow susceptibility assessment based on information value and machine learning coupling method: from the perspective of sustainable development. Environ. Sci. Pollut. Res., 17.

Chan, H.C., Chen, P.A., Lee, J.T., 2018. Rainfall-Induced Landslide Susceptibility Using a Rainfall-Runoff Model and Logistic Regression. Water 10, 18.

Chang, Z.L., Huang, F.M., Huang, J.S., Jiang, S.H., Liu, Y.T., Meena, S.R., Catani, F., 2023. An updating of landslide susceptibility prediction from the perspective of space and time. Geosci. Front. 14, 13.

Chen, C.I., Huang, S.J., 2013. The necessary and sufficient condition for GM(1,1) grey prediction model. Appl. Math. Comput. 219, 6152-6162.

Chen, L.F., Guo, H.X., Gong, P.S., Yang, Y.Y., Zuo, Z.L., Gu, M.Y., 2021. Landslide susceptibility assessment using weights-of-evidence model and cluster analysis along the highways in the Hubei section of the Three Gorges Reservoir Area. Comput. Geosci. 156, 13.

Chen, T., Zhu, L., Niu, R.Q., Trinder, C.J., Peng, L., Lei, T., 2020. Mapping landslide susceptibility at the Three Gorges Reservoir, China, using gradient boosting decision tree, random forest and information value models. J Mt. Sci. 17, 670-685.

Chen, W., Peng, J.B., Hong, H.Y., Shahabi, H., Pradhan, B., Liu, J.Z., Zhu, A.X., Pei, X.J., Duan, Z., 2018. Landslide susceptibility modelling using GIS-based machine learning techniques for Chongren County, Jiangxi Province, China. Sci. Total Environ. 626, 1121-1135.

Chen, W.T., Li, X.J., Wang, Y.X., Chen, G., Liu, S.W., 2014. Forested landslide detection using LiDAR data and the random forest algorithm: A case study of the Three Gorges, China. Remote Sens. Environ. 152, 291-301.

Cheng, J.Y., Dai, X.A., Wang, Z.K., Li, J.Z., Qu, G., Li, W.L., She, J.X., Wang, Y.L., 2022. Landslide Susceptibility Assessment Model Construction Using Typical Machine Learning for the Three Gorges Reservoir Area in China. Remote Sens. 14, 28.

Chung, M.C., Tan, C.H., Chen, C.H., 2017. Local rainfall thresholds for forecasting landslide occurrence: Taipingshan landslide triggered by Typhoon Saola. Landslides 14, 19-33.

Ciurleo, M., Mandaglio, M.C., Moraci, N., 2019. Landslide susceptibility assessment by TRIGRS in a frequently affected shallow instability area. Landslides 16, 175-188.

Cobos-Mora, S.L., Rodriguez-Galiano, V., Lima, A., 2023. Analysis of landslide explicative factors and susceptibility mapping in an andean context: The case of Azuay province (Ecuador). Heliyon 9, 17.

Dahal, R.K., Hasegawa, S., 2008. Representative rainfall thresholds for landslides in the Nepal Himalaya.

Geomorphology 100, 429-443.
Fan, X.L., Feng, X.F., Dong, Y.Y., Hou, H.C., 2022. COVID-19 CT image recognition algorithm based on transformer and CNN. Displays 72, 9.
Gariano, S.L., Supplizi, G.V., Ardizzone, F., Salvati, P., Bianchi, C., Morbidelli, R., Saltalippi, C., 2021. Long-term analysis of rainfall-induced landslides in Umbria, central Italy. Nat. Hazards 106, 2207-2225.
Gill, H.S., Khalaf, O.I., Alotaibi, Y., Alghamdi, S., Alassery, F., 2022. Multi-Model CNN-RNN-LSTM Based Fruit Recognition and Classification. Intell. Autom. Soft Comput. 33, 637-650.
Guo, B., Pei, X.J., Xu, M., Li, T.T., 2022. Analyzing Rainfall Threshold for Shallow Landslides Using Physically Based Modeling in Rasuwa District, Nepal. Water 14, 12.
Guo, Z.Z., Shi, Y., Huang, F.M., Fan, X.M., Huang, J.S., 2021. Landslide susceptibility zonation method based on C5.0 decision tree and K-means cluster algorithms to improve the efficiency of risk management. Geosci. Front. 12, 19.
Habumugisha, J.M., Chen, N.S., Rahman, M., Islam, M.M., Ahmad, H., Elbeltagi, A., Sharma, G., Liza, S.N., Dewan, A., 2022. Landslide Susceptibility Mapping with Deep Learning Algorithms. Sustainability 14, 22.
Hasan, M.M., Nilay, M.S.M., Jibon, N.H., Rahman, R.M., 2023. LULC changes to riverine flooding: A case study on the Jamuna River, Bangladesh using the multilayer perceptron model. Results Eng. 18, 19.
He, Q.F., Shahabi, H., Shirzadi, A., Li, S.J., Chen, W., Wang, N.Q., Chai, H.C., Bian, H.Y., Ma, J.Q., Chen, Y.T., Wang, X.J., Chapi, K., Bin Ahmad, B., 2019. Landslide spatial modelling using novel bivariate statistical based Naive Bayes, RBF Classifier, and RBF Network machine learning algorithms. Sci. Total Environ. 663, 1-15.
He, S.S., Wang, J., Liu, S.N., 2020. Rainfall Event-Duration Thresholds for Landslide Occurrences in China. Water 12, 17.
Hoffman, S., Jasinski, R., 2023. The Use of Multilayer Perceptrons to Model PM2.5 Concentrations at Air Monitoring Stations in Poland. Atmosphere 14, 19.
Huang, F.M., Cao, Z.S., Jiang, S.H., Zhou, C.B., Huang, J.S., Guo, Z.Z., 2020. Landslide susceptibility prediction based on a semi-supervised multiple-layer perceptron model. Landslides 17, 2919-2930.
Huang, F.M., Chen, J.W., Liu, W.P., Huang, J.S., Hong, H.Y., Chen, W., 2022a. Regional rainfall-induced landslide hazard warning based on landslide susceptibility mapping and a critical rainfall threshold. Geomorphology 408, 16.
Huang, F.M., Teng, Z.K., Yao, C., Jiang, S.H., Catani, F., Chen, W., Huang, J.S., 2024. Uncertainties of landslide susceptibility prediction: Influences of random errors in landslide conditioning factors and errors reduction by low pass filter method. J. Rock Mech. Geotech. Eng. 16, 213-230.
Huang, F.M., Yan, J., Fan, X.M., Yao, C., Huang, J.S., Chen, W., Hong, H.Y., 2022b. Uncertainty pattern in landslide susceptibility prediction modelling: Effects of different landslide boundaries and spatial shape expressions. Geosci. Front. 13, 16.
Jiang, P., Zeng, Z.G., Chen, J.J., Tang, H.M., Ieee, 2014. A PSOGSA method to optimize the T-S fuzzy neural network for displacement prediction of landslide, IEEE International Conference on Systems, Man, and Cybernetics (SMC). Ieee, San Diego, CA, pp. 1216-1221.
Jin, L., Li, Z.C., Tang, J.H., 2023. Deep Semantic Multimodal Hashing Network for Scalable Image-Text and Video-Text Retrievals. IEEE Trans. Neural Netw. Learn. Syst. 34, 1838-1851.
Kaliyar, R.K., Goswami, A., Narang, P., 2021. FakeBERT: Fake news detection in social media with a BERT-based deep learning approach. Multimed. Tools Appl. 80, 11765-11788.
Kumar, P.C.M., Kavitha, R., 2021. Prediction of nanofluid viscosity using multilayer perceptron and Gaussian process regression. J. Therm. Anal. Calorim. 144, 1151-1160.
Lee, M.L., Ng, K.Y., Huang, Y.F., Li, W.C., 2014. Rainfall-induced landslides in Hulu Kelang area, Malaysia. Nat. Hazards 70, 353-375.
Li, W.J., Fang, Z.C., Wang, Y., 2022. Stacking ensemble of deep learning methods for landslide susceptibility mapping in the Three Gorges Reservoir area, China. Stoch. Environ. Res. Risk Assess. 36, 2207-2228.
Li, Y.W., Wang, X.M., Mao, H., 2020. Influence of human activity on landslide susceptibility development in the Three Gorges area. Nat. Hazards 104, 2115-2151.
Lim, D.H., Na, W.J., Hong, W.H., Bae, Y.H., 2023. Development of a fire prediction model at the urban planning stage: Ordinary least squares regression analysis of the area of urban land use and fire damage data in South Korea. Fire Saf. J. 136, 8.

Liu, M.M., Liu, J.P., Xu, S.H., Chen, C., Bao, S., Wang, Z.L., Du, J., 2023. 3DCNN landslide susceptibility considering spatial-factor features. Front. Environ. Sci. 11, 12.

Liu, X., Yin, K., Xiao, C., Chen, L., Zeng, T., Li, Y., Liu, Z., Gong, Q., Chen, W., 2022. Meteorological early warning of landslide based on I-D-R threshold model. Earth Science, 1-15. (in Chinese).

Long, J.J., Liu, Y., Li, C.D., Fu, Z.Y., Zhang, H.K., 2021. A novel model for regional susceptibility mapping of rainfall-reservoir induced landslides in Jurassic slide-prone strata of western Hubei Province, Three Gorges Reservoir area. Stoch. Environ. Res. Risk Assess. 35, 1403-1426.

Marin, R.J., 2020. Physically based and distributed rainfall intensity and duration thresholds for shallow landslides. Landslides 17, 2907-2917.

Marin, R.J., Garcia, E.F., Aristizabal, E., 2020. Effect of basin morphometric parameters on physically-based rainfall thresholds for shallow landslides. Eng. Geol. 278, 16.

Martinovic, K., Gavin, K., Reale, C., Mangan, C., 2018. Rainfall thresholds as a landslide indicator for engineered slopes on the Irish Rail network. Geomorphology 306, 40-50.

Mathew, J., Babu, D.G., Kundu, S., Kumar, K.V., Pant, C.C., 2014. Integrating intensity-duration-based rainfall threshold and antecedent rainfall-based probability estimate towards generating early warning for rainfall-induced landslides in parts of the Garhwal Himalaya, India. Landslides 11, 575-588.

Mei, J.Q., Chen, W.Y., Li, B.Y., Li, S.X., Zhang, J., Yan, J., 2023. Adaptive fusion of multi-exposure images based on perceptron model. Appl. Math. Nonlinear Sci., 14.

Narimani, R., Jun, C.H.Y., De Michele, C., Gan, T.Y., Nezhad, S.M., Byun, J., 2023. Multilayer perceptron-based predictive model using wavelet transform for the reconstruction of missing rainfall data. Stoch. Environ. Res. Risk Assess. 37, 2791-2802.

Niu, R.Q., Wu, X.L., Yao, D.K., Peng, L., Ai, L., Peng, J.H., 2014. Susceptibility Assessment of Landslides Triggered by the Lushan Earthquake, April 20, 2013, China. IEEE J. Sel. Top. Appl. Earth Observ. Remote Sens. 7, 3979-3992.

Peruccacci, S., Brunetti, M.T., Gariano, S.L., Melillo, M., Rossi, M., Guzzetti, F., 2017. Rainfall thresholds for possible landslide occurrence in Italy. Geomorphology 290, 39-57.

Pradhan, A.M.S., Kang, H.S., Lee, J.S., Kim, Y.T., 2019. An ensemble landslide hazard model incorporating rainfall threshold for Mt. Umyeon, South Korea. Bull. Eng. Geol. Environ. 78, 131-146.

Rohan, T., Shelef, E., Mirus, B., Coleman, T., 2023. Prolonged influence of urbanization on landslide susceptibility. Landslides 20, 1433-1447.

Rossi, M., Luciani, S., Valigi, D., Kirschbaum, D., Brunetti, M.T., Peruccacci, S., Guzzetti, F., 2017. Statistical approaches for the definition of landslide rainfall thresholds and their uncertainty using rain gauge and satellite data. Geomorphology 285, 16-27.

Salee, R., Chinkulkijniwat, A., Yubonchit, S., Horpibulsuk, S., Wangfaoklang, C., Soisompong, S., 2022. New threshold for landslide warning in the southern part of Thailand integrates cumulative rainfall with event rainfall depth-duration. Nat. Hazards 113, 125-141.

Sarkar, S., Chandna, P., Pandit, K., Dahiya, N., 2023. An event-duration based rainfall threshold model for landslide prediction in Uttarkashi region, North-West Himalayas, India. Int. J. Earth Sci., 17.

Segoni, S., Tofani, V., Rosi, A., Catani, F., Casagli, N., 2018. Combination of Rainfall Thresholds and Susceptibility Maps for Dynamic Landslide Hazard Assessment at Regional Scale. Front. Earth Sci. 6, 11.

Selamat, S.N., Abd Majid, N., Taha, M.R., Osman, A., 2022. Landslide Susceptibility Model Using Artificial Neural Network (ANN) Approach in Langat River Basin, Selangor, Malaysia. Land 11, 21.

Sheng, Y.F., Li, Y.Y., Xu, G.L., Li, Z.G., 2022. Threshold assessment of rainfall-induced landslides in Sangzhi County: statistical analysis and physical model. Bull. Eng. Geol. Environ. 81, 15.

Soralump, S., Shrestha, A., Thowiwat, W., Sukjaroen, R., Chaithong, T., Yangsanphu, S., Koirala, A., Jotisankasa, A., 2021. Assessment of landslide behaviour in colluvium deposit at Doi Chang, Thailand. Sci Rep 11, 12.

Teja, T.S., Dikshit, A., Satyam, N., 2019. Determination of Rainfall Thresholds for Landslide Prediction Using an Algorithm-Based Approach: Case Study in the Darjeeling Himalayas, India. Geosciences 9, 9.

Wang, C., Wang, X.D., Zhang, H.Y., Meng, F.Q., Li, X.L., 2023a. Assessment of environmental geological disaster susceptibility under a multimodel comparison to aid in the sustainable development of the regional economy. Environ. Sci. Pollut. Res. 30, 6573-6591.

Wang, X.B., Zhao, Y.Q., Li, W.F., 2023b. Recognition of Commercial Vehicle Driving Cycles Based on Multilayer Perceptron Model. Sustainability 15, 21.

Wang, X.L., Zhang, L.Q., Wang, S.J., Lari, S., 2014. Regional landslide susceptibility zoning with considering the aggregation of landslide points and the weights of factors. Landslides 11, 399-409.

Wang, X.N., Zhang, X.L., Bi, J., Zhang, X.D., Deng, S.Q., Liu, Z.W., Wang, L.Z., Guo, H.X., 2022a. Landslide Susceptibility Evaluation Based on Potential Disaster Identification and Ensemble Learning. Int. J. Environ. Res. Public Health 19, 26.

Wang, Z.Y., Ma, C.M., Qiu, Y., Xiong, H.X., Li, M.H., 2022b. Refined Zoning of Landslide Susceptibility: A Case Study in Enshi County, Hubei, China. Int. J. Environ. Res. Public Health 19, 22.

Wu, C.Y., Yeh, Y.C., 2020. A Landslide Probability Model Based on a Long-Term Landslide Inventory and Rainfall Factors. Water 12, 17.

Wu, Y.M., Lan, H.X., Gao, X., Li, L.P., Yang, Z.H., 2015. A simplified physically based coupled rainfall threshold model for triggering landslides. Eng. Geol. 195, 63-69.

Xia, P., Hu, X.L., Wu, S.S., Ying, C.Y., Liu, C., 2020. Slope Stability Analysis Based on Group Decision Theory and Fuzzy Comprehensive Evaluation. J. Earth Sci. 31, 1121-1132.

Xing, X.F., Wu, C.L., Li, J.H., Li, X.Y., Zhang, L.M., He, R.J., 2021. Susceptibility assessment for rainfall-induced landslides using a revised logistic regression method. Nat. Hazards 106, 97-117.

Yang, H.J., Wei, F.Q., Ma, Z.F., Guo, H.Y., Su, P.C., Zhang, S.J., 2020. Rainfall threshold for landslide activity in Dazhou, southwest China. Landslides 17, 61-77.

Yang, Z.Q., Xu, C., Shao, X.Y., Ma, S.Y., Li, L., 2022. Landslide susceptibility mapping based on CNN-3D algorithm with attention module embedded. Bull. Eng. Geol. Environ. 81, 21.

Youssef, A.M., Pradhan, B., Dikshit, A., Al-Katheri, M.M., Matar, S.S., Mahdi, A.M., 2022. Landslide susceptibility mapping using CNN-1D and 2D deep learning algorithms: comparison of their performance at Asir Region, KSA. Bull. Eng. Geol. Environ. 81, 22.

Yu, L.B., Zhou, C., Wang, Y., Cao, Y., Peres, D.J., 2022. Coupling Data- and Knowledge-Driven Methods for Landslide Susceptibility Mapping in Human-Modified Environments: A Case Study from Wanzhou County, Three Gorges Reservoir Area, China. Remote Sens. 14, 21.

Yuniawan, R.A., Rifa'i, A., Faris, F., Subiyantoro, A., Satyaningsih, R., Hidayah, A.N., Hidayat, R., Mushthofa, A., Ridwan, B.W., Priangga, E., Muntohar, A.S., Jetten, V.G., van Westen, C.J., den Bout, B.V., Sutanto, S.J., 2022. Revised Rainfall Threshold in the Indonesian Landslide Early Warning System. Geosciences 12, 17.

Zhang, H., Yin, C., Wang, S.P., Guo, B., 2022. Landslide susceptibility mapping based on landslide classification and improved convolutional neural networks. Nat. Hazards, 41.

Zhang, J.Y., Ma, X.L., Zhang, J.L., Sun, D.L., Zhou, X.Z., Mi, C.L., Wen, H.J., 2023. Insights into geospatial heterogeneity of landslide susceptibility based on the SHAP-XGBoost model. J. Environ. Manage. 332, 20.

Zhao, B.R., Dai, Q., Han, D.W., Dai, H.C., Mao, J.Q., Zhuo, L., 2019. Probabilistic thresholds for landslides warning by integrating soil moisture conditions with rainfall thresholds. J. Hydrol. 574, 276-287.

Zhao, L.H., Liu, M., Song, Z.C., Wang, S.G., Zhao, Z.G., Zuo, S., 2022. Regional-scale modeling of rainfall-induced landslides under random rainfall patterns. Environ. Modell. Softw. 155, 14.

Zhou, C., Cao, Y., Hu, X., Yin, K.L., Wang, Y., Catani, F., 2022. Enhanced dynamic landslide hazard mapping using MT-InSAR method in the Three Gorges Reservoir Area. Landslides 19, 1585-1597.

Zhu, C.H., Hu, G.D., 2012. Time Series Prediction of Landslide Displacement Using SVM Model: Application to Baishuihe Landslide in Three Gorges Reservoir Area, China, International Conference on Measurement, Instrumentation and Automation (ICMIA 2012). Trans Tech Publications Ltd, Guangzhou, PEOPLES R CHINA, pp. 1413-+.